Interleukin-2 shapes the cytotoxic T cell proteome and immune environment sensing programs

Rollings, Christina; Sinclair, Linda; Brady, Hugh J. M. ; Cantrell, Doreen; Ross, Sarah

Published in:
Science Signaling

DOI:
10.1126/scisignal.aap8112

Publication date:
2018

Document Version
Peer reviewed version

Title: Interleukin-2 shapes the cytotoxic T cell proteome and immune-environment sensing programs

Authors: Christina M. Rollings[1], Linda V. Sinclair[1], Hugh J. M. Brady[2], Doreen A. Cantrell[1*] and Sarah H. Ross[1*]

Affiliations:

[1]Division of Cell Signalling and Immunology, School of Life Sciences, University of Dundee, DD1 5EH, United Kingdom.

[2]Department of Life Sciences, Imperial College London, London, SW7 2AZ, UK.

*Correspondence should be addressed to D. A. Cantrell (d.a.cantrell@dundee.ac.uk) or S. H. Ross (s.t.ross@dundee.ac.uk).

One Sentence Summary:

Interleukin-2 controls the protein composition of T cells to regulate their responses to environmental stimuli.

Abstract:

Interleukin-2 (IL-2) and Janus kinases (JAKs) regulate transcriptional programs and protein synthesis to control the protein content and biomass of effector $CD8^+$ cytotoxic T cell (CTL) differentiation. Using high-resolution mass spectrometry, we have generated an in-depth characterisation of how IL-2 and JAKs configure the CTL proteome. We found that IL-2-JAK1/3 signaling selectively regulated protein expression, influencing the levels of critical cytokines and effector molecules in T cells. Moreover, IL-2 controlled the expression of proteins that support core metabolic processes essential for cellular fitness. One fundamental insight was the dominant role for IL-2 in controlling how effector T cells respond to their microenvironment. IL-2-JAK1/3 signaling pathways thus controlled abundance of nutrient transporters, nutrient sensors and critical oxygen sensing molecules. These data provide key insights of how IL-2 controls T cell function and highlight signaling mechanisms and transcription factors that link oxygen sensing to transcriptional control of $CD8^+$ T cell differentiation.

Main Text:

Introduction

Interleukin-2 (IL-2), a member of the γ_c chain cytokine family, has numerous roles in orchestrating immune responses, including controlling the proliferation and differentiation of $CD4^+$ and $CD8^+$ effector T cells *(1-5)*. This vital role in controlling T cell function and fate has made manipulation of IL-2 signaling an attractive aim for immunotherapies. Hence, IL-2 was one of the first cytokines used in immunotherapy to increase T cell responses. IL-2 is also used to expand tumor-specific T cells and chimeric antigen receptor redirected T cells (CAR-T cells) ex vivo before adoptive transfer to patients *(6, 7)*. IL-2 signals via the tyrosine kinases JAK1 and JAK3, and, hence, JAK1/3-specific inhibitors such as Tofacitinib have been developed to modulate IL-2 immunoregulatory pathways to treat autoimmune and inflammatory conditions. Moreover, the pleiotropic role of IL-2 in controlling both pro-inflammatory effector T cell responses and the anti-inflammatory homeostasis of regulatory T cells has stimulated the development of strategies using modified IL-2 proteins with altered receptor binding *(8)* and anti-cytokine antibodies *(4, 9)* to manipulate IL-2 signaling responses for therapies.

In terms of $CD8^+$ cytotoxic T lymphocytes (CTL), IL-2 was first studied because of its ability to drive T cell growth and T cell clonal expansion *(6, 10, 11)*. IL-2, thus, regulates expression of transcriptional programs that are required for cell cycle progression and proliferation. IL-2 also controls the production of interferon gamma (IFNγ) and perforin/granzyme effector molecules and regulates the expression of adhesion molecules and chemokine receptors that dictate the balance of cell trafficking to secondary lymphoid organs or peripheral tissues. IL-2 can, thus, direct

effector CTL differentiation at the expense of memory $CD8^+$ T cell development *(12-15)*. The best characterized IL-2-induced gene transcriptional programs are mediated by signal transducer and activator of transcription 5 (STAT5) proteins *(3, 16-18)* and by MYC *(19)*.

However, IL-2-JAK1/3 control of serine/threonine kinase signaling networks is also very important. For example, IL-2 controls the activity of mammalian target of rapamycin complex 1 (mTORC1)-mediated signaling pathways that regulate the expression of inflammatory cytokines, cytolytic effector molecules, glucose transporters and glucose and fatty acid metabolism in CTL *(20-23)*. The IL-2-JAK-regulated phosphoproteome of CTL is dominated by proteins that regulate mRNA stability and protein translational machinery *(24)*. Moreover, a key role for IL-2 is to sustain protein synthesis in CTL allowing IL-2 to act as a potent 'growth factor' for immune activated T cells *(12, 24, 25)*. The ability to control protein synthesis *(24, 25)* allows IL-2 to modify the proteome of CTLs independently of the transcriptional program. One example of this is IL-2 control of the expression of the transcription factor MYC, where the dominant role of IL-2 is to regulate the synthesis of MYC protein independently of its mRNA *(19)*. Furthermore, IL-2-regulation of mTORC1, which can control mRNA translation and cellular protein degradation pathways *(23)*, is another means by which IL-2 may regulate cellular proteomes independently of transcriptional programs.

The direct action of IL-2 is to activate JAK kinases, but understanding the full consequences of how IL-2 controls T cell function requires IL-2-dependent proteomes to be mapped. Accordingly, we have used high resolution quantitative mass

spectrometry to analyze how IL-2 regulates the CTL proteome to generate global and in-depth insights into how this key cytokine controls $CD8^+$ T cell identity and controls cell cycle progression, metabolism and expression of effector molecules.

Results

IL-2 regulation of the CTL proteome

To explore the role of IL-2 on effector $CD8^+$ cytotoxic T lymphocyte (CTL) function, we used IL-2 differentiated effector $CD8^+$ T cells from P14 TCR transgenic mice. IL-2 maintained CTL are large granular cells (Fig. 1A) that depend on IL-2 for sustained proliferation and viability. After 24 hours of IL-2 deprivation, CTL had similar viability to the IL-2 maintained cultures (Fig. 1A), but were decreased in size, as judged by flow cytometry forward scatter (Fig. 1A). After 48 hours of IL-2 deprivation, cell viability had substantially decreased. The decrease in cell size of IL-2 deprived CTL observed by flow cytometry at the 24 hour time point (Fig. 1A) correlated with a reduction in CTL mass (Fig. 1B). Thus, to understand how IL-2 shapes the CTL phenotype, we used quantitative label-free high-resolution mass spectrometry to compare the proteome of CTL maintained in IL-2 and CTL deprived of IL-2 for 24 hours. For these experiments, CTL were lysed in urea and digested with LysC and trypsin. Peptides were fractionated using strong anion exchange (SAX) chromatography before analysis with an LTQ-Orbitrap Velos mass spectrometer. MaxQuant was used to identify and quantify proteins (Supplementary Fig. S1A).

Over 6200 protein groups were identified per biological replicate (Supplementary Fig. S1B- S1C and Supplementary Table S1) and there was >90% overlap in the proteins identified between the 3 biological replicates (Supplementary Fig. S1B-S1C). We

converted our label-free data into protein copy numbers per cell using "histone-ruler" methodology *(26)*. The correlation between estimated copy numbers of proteins in different biological replicates of each condition was good, with the lowest r^2-value being 0.90 (Supplementary Fig. S1D-S1E).

IL-2 deprived CTL decreased in size (Fig. 1A) and mass (Fig. 1B) compared to IL-2 maintained CTL. Hence a key question was whether IL-2 removal resulted in an equal and uniform reduction in all proteins in CTL. In total, ~6500 proteins were identified in both IL-2 maintained CTL and IL-2-deprived CTL (Fig. 1C) with protein expression spanning several orders of magnitude. A key result was that ~3000 proteins were not significantly affected by the loss of IL-2: this included cytoskeletal and structural proteins, such as b-actin (ACTB), one of the most highly abundant proteins in CTL, vimentin and laminin-b and signaling molecules, such as PTPN6 (SHP-1), PTPN22 and RAP1B (Supplementary Table S1). A further indication that loss of IL-2 signals did not result in a universal loss in protein was that the expression of a few proteins significantly increased by IL-2 deprivation (Fig. 1C).

Approximately 100 proteins, including ribosomal proteins, glycolytic enzymes and the cytolytic effector molecules, Granzyme A and Granzyme B, contributed to ~50% of the mass of IL-2 maintained CTL (Fig. 1D). Therefore, IL-2 could control cell mass by regulating only the expression of abundant proteins. The overall reduction in mass of a CTL deprived of IL-2 was between 1.5-2-fold (Fig. 1B), and while this included the loss of some of the abundant proteins, the impact of IL-2 deprivation on the CTL proteome was complex. We found ~900 proteins that decreased proportionally to the overall loss in mass, indicative of some general cell scaling

down of protein content. However, the majority of IL-2 regulated proteins were changed in expression by more than 2-fold (Fig. 1C and Supplementary Table S2). The expression of a subset of CTL proteins was also highly sensitive to IL-2 deprivation; there was a complete loss of ~140 proteins, and changes in expression of other proteins of >20-fold. The effect of IL-2 on CTL cell mass is, thus, not just a simple reduction and scaling down in overall cellular protein content, but a more complex reshaping of the proteome.

Dominant effects of IL-2 on the CTL proteome

To understand the most dominant consequences of IL-2 deprivation on the CTL proteome, we focused on the proteins that were most decreased by loss of IL-2. Approximately 140 proteins were only reproducibly identified in IL-2 maintained CTL: these proteins included the effector cytokines, lymphotoxin α (LT-α), and IFNγ (Supplementary Table S2). Interestingly, TNFRSF9 (CD137 or 4-1BB) is one of the most down regulated proteins in CTL deprived of IL-2, going from ~300, 000 molecules per cell in IL-2 maintained CTL to ~2000 molecules per cell in the absence of IL-2 (Supplementary Table S2). Other examples of cell surface receptors strongly regulated by IL-2 include the IL-4R, IL-12β1 and the inhibitory receptor, Tim-3 (HAVCR2) (Fig. 1E). Previous studies have shown that the expression of the IL-2Rα (CD25) is controlled by IL-2 *(27)* and we identified a 2-5-fold reduction in the expression of IL-2Rα (CD25) following IL-2 deprivation of CTL (Fig. 1F). This decrease was consistent with the observed changes to CD25 as determined by flow cytometry analysis of the CTL prior to their proteomic analysis (Fig. 1G). We also noted that IL-2Rβ and IL-2Rγ, the other components of the IL-2 receptor, were decreased in IL-2 deprived CTL (Fig. 1E). Collectively, the proteomic data

highlighted the key role for IL-2 in sustaining the expression of proteins that allow CTL to respond to exogenous cytokines and inhibitory receptor stimuli.

IL-2 regulation of cell cycle machinery

A quintessential biological function of IL-2 is to control the clonal expansion of antigen receptor-activated T cells. The commitment of T cells to DNA synthesis is known to be dependent on the activity of cyclin D-CDK2 or cyclin D-CDK4 complexes. Our data allowed us to quantitate the impact of IL-2 deprivation on the numbers and stoichiometry of the key cell cycle regulators to fully understand how IL-2 regulates T cell proliferation. We found that IL-2 positively regulated the expression of cyclin D2 (Fig. 1H) and cyclin D3 (Fig. 1I). Conversely, IL-2 suppressed expression of the CDK inhibitor CDKN1B (p27kip) (Fig. 1J). In terms of copy numbers per cell, IL-2 deprived CTL showed increased levels of CDKN1B molecules relative to the numbers of cyclins D2 and D3 molecules (Fig 1K). This would result in decreased levels of active cyclin D/CDK complexes and would be consistent with inhibition of G1/S cell cycle progression. However, our data also revealed that IL-2 deprivation caused a decrease in expression of essential components of the DNA replication machinery (Fig. 1L) which would further impact on the ability of CTL to perform DNA synthesis. Another interesting insight from our data was that IL-2 sustained the expression of DNA damage repair proteins (Fig. 1L). As CDK4/6-cyclin D complexes can control the activity of E2F and the synthesis of DNA replication proteins *(28)*, it could be that loss of the core DNA synthesis machinery is a consequence of loss of CDK4/6-cyclin D activity. There are, thus, multiple mechanisms by which loss of IL-2 signals influence DNA synthesis and repair in effector T cells to control T cell cycle progression and proliferation.

IL-2 regulation of the CTL cytolytic machinery

The key cytolytic effector molecules of CTL are perforin, granzymes, and FAS ligand which are stored in granules which are specialized secretory lysosomes marked by expression of LAMP-1 (CD107a) and LAMP-2 *(29)*. IL-2 only had a minor effect on LAMP1/2 expression in CTL, indicating that IL-2 loss did not significantly decrease the lysosomal content of the CTL (Fig. 2A-2B). However, IL-2 did influence the expression of cytolytic granule cargo molecules, notably perforin, but also granzyme A and B (Fig. 2C-2E). IL-2 also regulated expression of some essential regulators of cytolytic granule fusion with the plasma membrane such as RAB27A, STXBP2 (MUNC18-2) and UNC13D (MUNC13-4) (Fig. 2F-2H). IL-2, thus, has the potential to regulate the protein content and release of lytic granules.

IL-2 control of transcriptional regulators and core protein synthesis machinery

Another key function of IL-2 is to regulate and maintain T cell transcriptional programs, in part via regulation of STAT5. Our data showed that IL-2 could have a significant influence on gene transcription, and hence mRNA production, in CTL by controlling the expression of multiple transcription factors (Fig. 3A). Moreover, histone and DNA methylases, DNA and RNA helicases and RNA processing proteins were all decreased in CTL in the absence of IL-2 (Fig. 3A). Indeed, some abundant transcription factors were potently regulated by IL-2 (Fig. 3A and Supplementary Table S2). These included ETS translocation variant 3 (ETVS3), MAFK, NFIL3 AP-1 family proteins JUN, JUNB, JUND and FOSL2 (Fig. 3A). IL-2 also controlled Eomesodermin (EOMES), IRF8 and TCF25 expression (Fig. 3B). However, the expression of two crucial T cell transcription factors FOXO1 (Fig. 3C) and TBET (Fig. 3C) were not significantly changed by loss of IL-2 signals. These data highlight

that the ability of IL-2 to control gene transcription and the production and stability of mRNAs in T cells goes beyond control of STAT5 phosphorylation and activity.

The phenotype of a cell is controlled by its transcriptional program but gene expression cannot be executed without protein synthesis. It has been shown that IL-2 has a key role in regulating rates of protein synthesis in $CD8^+$ T cells *(24, 25)* but the molecular basis for this is not understood. The proteomic analysis revealed that IL-2 influenced protein synthesis on many levels. IL-2 controlled the expression of ribosomal proteins (Fig. 3D and 3E). In terms of ribosome copy number, CTL express ~2.8×10^6 ribosomes and this reduces to ~1.2×10^6 ribosomes in IL-2 deprived cells. IL-2 also controlled expression of tRNA synthases, including the methionyl-tRNA synthase (Fig. 3E) and sustained the expression of critical components of the EIF translational initiation complex (Fig. 3E). Interestingly, IL-2 supported expression of proteins that regulate the transport of newly synthesized proteins into the ER and controlled expression of molecules that control protein folding and pathways of protein degradation in the ER lumen (Fig. 3E). These data reveal that IL-2 co-ordinates expression of ribosomes, translation complexes and protein quality control pathways.

IL-2 regulation of amino acid transporters and amino acid sensors

A maintained supply of amino acids is required in order for cells to sustain high rates of protein synthesis. We have previously shown that IL-2 controls System L mediated amino acid transport in CTL *(30)*. Moreover, $CD8^+$ T cells that lack expression of the system L amino acid transporter SLC7A5 fail to differentiate into CTL *(30)*. Our proteomics data showed that SLC7A5 is the most abundant amino acid transporter in

CTL expressed at ~170 000 copies per cell and that its expression was dependent on IL-2 (Fig. 4A). We also identified and quantitated expression of ~10 other amino acid transporters in CTL including transporters for arginine (SLC7A1) (Fig. 4B) and glutamine and serine (SLC1A5) (Fig. 4C). Strikingly, the expression of amino acid transporters was controlled by IL-2 (Fig. 4D). It was also of note that IL-2 regulated the expression of proteins required for amino acid biosynthesis (Fig. 4E) and the recovery of amino acids by autophagy (Fig. 4F- 4I). IL-2, thus, controls the supply of amino acids to CTL by multiple mechanisms.

A source of amino acids is vital for the protein biosynthetic capacity of T cells, but also controls other essential metabolic processes. For example, serine fuels the biosynthesis of purine nucleotides needed for T cell proliferation *(31)*; glutamine fuels critical protein O-GlcNAcylations in T cells *(32)*; intracellular levels of arginine control the metabolic fitness and survival of T cells *(33)* and, together with leucine, regulate the activity of mTORC1. Signals mediated by mTORC1 are critical for controlling the differentiation of $CD8^+$ T cells *(20-22)*. The ability of IL-2 to control the supply of leucine and arginine affords insights as to how IL-2 can sustain high level of mTORC1 activity in effector CTL. However, other new insights are that IL-2 controls the expression of amino acid sensing and regulatory proteins that direct mTORC1 activity *(34)* (Fig. 4J-4L). IL-2, hence, drives expression of the cytosolic leucine sensor SESTRIN2 (Fig. 4K) and the GTPase RHEB (Fig. 4L). IL-2, thus, regulates amino acid-dependent activation of mTORC1 in two ways; by regulating the supply of amino acids and by controlling the abundance of amino acid-sensing pathways.

IL-2 control of glucose metabolism and oxygen sensing

CTL have high rates of glucose transport, are highly glycolytic and have high rates of oxidative phosphorylation and need to sustain these metabolic programs for effector function *(23)*. In our dataset, we found that proteins mapped to oxidative phosphorylation comprised ~1% of the IL-2-maintained CTL proteome by mass (Fig. 5A), proteins of the TCA cycle were ~0.8% of the CTL proteome (Fig. 5B), and ~9% of the CTL proteome consisted of glycolytic enzymes (Fig. 5C). IL-2 deprivation did scale down the proteins involved glucose metabolism but they remained highly expressed and at a similar relative abundance (Fig. 5A-5C). However, the rate limiting step for glucose metabolism in CTL is glucose transport, and our data demonstrated that IL-2 controls expression of the glucose transporters GLUT1 (SLC2A1) and GLUT3 (SLC2A3) in CTL (Fig. 5D-5E). The relevance of the changes in glucose transporter expression is evidenced by the decrease in the glucose transport capacity of IL-2 deprived CTL compared to CTL maintained in IL-2 (Fig. 5F).

The expression of glucose transporters in CTL is controlled by the HIF1α/HIF1β transcriptional complex *(21)*. IL-2 deprivation caused a decreased expression of HIF1β (Fig. 5G) and HIF1α (Fig. 5H) *(21)*. We have previously described HIF1 target genes in CTL *(21)* and our data showed that in addition to the loss of GLUT1 and GLUT3, other transcriptional targets for HIF1, such as perforin (Fig. 2C), the inhibitory receptor, Tim-3 (HAVCR2) (Fig. 5I) and NFIL3 (Fig. 5J) were decreased upon IL-2 deprivation. Additionally, we have previously established that HIF1 complexes repress expression of the cell adhesion molecule, CD62L (L-selectin) *(21)*. The increased expression of CD62L (Fig. 5K) in IL-2 deprived CTL was thus also consistent with the loss of the HIF transcriptional program.

In CTL, the expression of HIF1α is promoted by the activity of the mTORC1 pathway *(21)*. In the presence of high oxygen, the oxygen-dependent proline hydroxylase (PHD) proteins hydroxylate prolines within HIF1α, targeting HIF1α for ubiquitination by the VHL ubiquitin ligase. This limits the levels of HIF1α in CTL when oxygen levels are high but allows very tight upregulation of HIF1α expression in response to changes in the oxygen environment. The importance these oxygen sensing pathways mediated by PHD proteins and VHL in restraining $CD8^+$ T cell immune responses is being increasingly recognized *(35)*. We identified PHD2 as the dominant proline hydroxylase in CTL and did not detect PHD1 or PHD3. The expression of PHD2 was IL-2-regulated (Fig. 5L), highlighting IL-2 is a critical regulator of oxygen sensing signaling pathways in CTL.

IL-2 controls the CTL proteome via JAK kinases

IL-2-induced activation of JAK1 and JAK3 are essential for IL-2 signal transduction. Accordingly, a prediction is that pharmacological inhibition of JAKs would mimic the effect of IL-2 deprivation and re-shape the CTL proteome. We tested this prediction by using mass spectrometry to compare the proteome of CTL maintained in IL-2 alone or IL-2 in the presence of the JAK1/3 inhibitor, Tofacitinib, which is now used clinically to modify JAK1/3 activity in autoimmune diseases. In these experiments, we treated CTL with 100 nM of Tofacitinib, within the range of Tofacitinib levels found in plasma when this drug is used therapeutically *(36-39)*. Moreover, 100 nM Tofacitinib is sufficient to downregulate the tyrosine phosphorylation of STAT5 in CTL (Fig. 6A) *(24)* and is sufficient to prevent T cell cycle progression (Fig. 6B), suppress protein synthesis *(24)* and decrease the size (Fig. 6C) and protein content of CTL (Fig. 6D). Importantly, T cells treated with 100 nM Tofacitinib are viable after

24 hours of treatment; higher levels of the drug cause losses in cell viability. In the experiments with Tofacitinib, ~7000 protein groups were identified in the IL-2 maintained control and Tofacitinib treated CTL (Supplementary Fig. S2A-S2B and Supplementary Table S3). In each of these datasets, there was good correlation and over 87% overlap in the identified proteins between the replicates of each condition (Supplementary Fig. S2A-S2D). Inhibition of the JAK kinases had a less dramatic effect on the CTL proteome than IL-2 deprivation, but Tofacitinib treatment mirrored multiple aspects of the effect of IL-2 deprivation on the CTL proteome. For example, JAK1/3 inhibition caused loss of the cell surface proteins CD25 (Fig. 6F-6G), IL-4Rα, IL-12Rβ1 and TNFRSF9 (4-1BB/CD137) (Fig. 6E).

The expression of key cell cycle regulatory proteins and DNA synthesis machinery was also controlled by JAK1/3 (Fig. 7A). Tofacitinib treatment also replicated the effect of IL-2 removal on protein synthesis machinery and regulated proteins involved in ribosome biosynthesis and caused a reduction in the ribosome proteins (Fig. 7A). Inhibition of JAK1/3 mimicked the effect of IL-2 deprivation on the expression of amino acid transporters (Fig. 7B) and, like IL-2 deprivation, CTL treated with Tofacitinib decreased the expression of the mTORC1 pathway leucine sensor, Sestrin-2 (Fig. 7C). Tofacitinib treatment of CTL also decreased expression of the HIF1 targets, GLUT1 and GLUT3 (Fig. 7D-7E). This correlated with Tofacitinib-treated CTL having reduced glucose uptake (Fig. 7F) and glycolysis, as judged by lactate output (Fig. 7G) compared to IL-2 maintained CTL. Tofacitinib treated CTL also lost expression of other HIF targets such as perforin (Fig. 7H) and the NFIL3 transcription factor (Fig. 7I). This dependency of HIF1α expression on JAK activity was confirmed by immunoblot analysis with selective HIF1α antibodies (Fig. 7J). Collectively, these

data highlight how the ability of IL-2 to shape the T cell proteome is dependent on JAK catalytic activity; the data also give pertinent information about the extent to which a clinically relevant inhibitor of JAK signaling modulates T cell responses to IL-2.

New insights about oxygen sensing pathways and the control of CTL transcriptional programs

A challenge with large, unbiased datasets is identifying data that give genuine new biological insights. In the current study, one strategy was to focus on molecules that had the largest change in protein expression in IL-2 deprived or Tofacitinib treated CTL. Another filter was to focus on molecules identified previously by our experiments mapping critical signaling pathways mediated by mTORC1 and HIF1 complexes in CTL *(21, 23)*. If these two filters were applied, then the transcriptional factor NFIL3 emerged as major target for IL-2-JAK1/3-mTORC1-HIF1 signaling. Our proteomics data, thus, indicated that NFIL3 was dramatically decreased in copy number (Fig. 5J and 7I) and relative abundance (Fig. 8A) in CTL in response to IL-2 deprivation or Tofacitinib treatment. These results were orthogonally validated by western blot analysis, showing that NFIL3 was lost in response to IL-2 deprivation or Tofacitinib treatment (Fig. 8B). IL-2 deprivation and Tofacitinib treatment also decreased the relative amount of NFIL3 mRNA (Fig. 8C), suggesting transcriptional regulation of NFIL3 contributes to its sustained expression in IL-2 maintained CTL.

NFIL3 has critical functions in NK cells *(40)*, $CD4^+$ T cells *(41)* and innate lymphoid cells (ILC) *(42)* but has not been previously reported to be expressed in $CD8^+$ T cells. Therefore, we evaluated the expression levels of NFIL3 at the protein and transcript

level in naïve and antigen activated P14 $CD8^+$ T cells. We found that NFIL3 protein and mRNA was undetectable in naïve $CD8^+$ T cells (Fig. 8D-8E) and low, albeit detectable, in antigen receptor activated T cells (Fig. 8D-8E). However, when antigen activated $CD8^+$ T cells were clonally expanded in IL-2 to produced effector CTL the levels of NFIL3 mRNA and protein increased and were sustained at high levels (Fig. 8D-8E). This is consistent with the model that NFIL3 expression is not TCR regulated but is dependent on IL-2-JAK1/3 signaling. Our proteomic data indicated that the expression of NFIL3 expression is dependent on mTORC1 activity *(23)*. We, thus, used immunoblot analysis and validated that the expression of NFIL3 in IL-2 maintained CTL is dependent on JAK1/3 signaling and mTORC1 signaling (Fig. 8F).

What about the role of oxygen sensing pathways in the control of NFIL3 expression? Affymetrix microarray analysis found that NFIL3 mRNA was decreased in HIF1β null CTL *(21)*. We, thus, evaluated NFIL3 levels in HIF1α null ($HIF1\alpha^{-/-}$) CTL. We found that NFIL3 expression in effector CTL was absolutely dependent on HIF1α expression (Fig. 8G). We also explored whether NFIL3 expression was increased if T cells were switched from 20% oxygen to 1% oxygen as this is known to increase expression of HIF1α and its target genes, including the glucose transporter GLUT1 (SLC2A1) and perforin *(21)*. We found that NFIL3 protein expression increased when wild-type but not $HIF1\alpha^{-/-}$ CTL were switched from 20% oxygen to 1% O_2 (Fig. 8G). This correlates with an increase in NFIL3 mRNA in CTL cultured in 1% O_2 compared to CTL cultured in 20% O_2 (Fig. 8H). This effect is comparable to the effect of the oxygen switch on expression of GLUT1 (Fig. 8I). Collectively, these data show that the expression of NFIL3 in CTL is regulated by oxygen sensing pathways controlled by the HIF1 transcription factor complex.

Is this regulation of NFIL3 in CTL important? To explore this question, $CD8^+$ naïve T cells from the spleens of $NFIL3^{-/-}$ deficient mice were TCR activated and clonally expanded in IL-2. $NFIL3^{-/-}$ $CD8^+$ T cells activated normally in response to TCR, and proliferated in response to IL-2 (Supplementary Fig. S3A). Moreover, IL-2 maintained $NFIL3^{-/-}$ $CD8^+$ effector T cells had normal levels of IL-2Rα and activation markers such as CD25, CD69 and CD44 (Supplementary Fig. S3B-S3D). They also showed normal activity of AKT and mTORC1, key regulators of CTL differentiation (Supplementary Fig. S3E-S3F). We have previously reported that HIF1 null effector $CD8^+$ T cells fail to downregulate expression of CD62L, a key adhesion molecule that controls lymphocyte migration into secondary lymphoid tissue, and do not express perforin *(21)*. $NFIL3^{-/-}$ $CD8^+$ T cells phenocopied HIF1α null $CD8^+$ T cells and retained high levels of expression of CD62L mRNA and protein (Fig. 8J-8K) and failed to express perforin mRNA and protein (Fig. 8L-8M). Collectively, these data identify NFIL3 as a transcription factor whose expression is regulated by mTORC1 and HIF1-mediated oxygen sensing pathways. They also show that NFIL3 controls perforin expression in T cells and has a role to repress expression of CD62L in immune activated $CD8^+$ T cells.

Discussion

The present study provides an in-depth understanding of how the proteome of effector $CD8^+$ T cells can be shaped by IL-2-JAK1/3 signaling. Our data uncover novel insights into the IL-2 regulated cellular processes and proteins that control differentiation and function of these key effector cells. One key perspective from the proteomic analysis was the extent to which IL-2-JAK1/3 signaling controls the ability of effector T cells to respond to their immune environment. IL-2 controls expression

of multiple cell surface molecules including receptors for the cytokines IL-4 and IL-12, the inhibitory receptor, Tim-3 (HAVCR2) and the co-stimulatory receptor, 4-1BB. The signaling pathways controlled by these receptors can modulate T cell responses powerfully. Indeed, a 4-1BB agonist antibody, Utomilumab, is in clinical trials to promote effector $CD8^+$ anti-tumor T cell therapy. The recognition that the expression of 4-1BB is tightly regulated by IL-2 is a useful insight into how therapeutic IL-2 treatments may be able to boost the function of effector T cells.

A further insight from our data was that IL-2 maintains the expression of proteins that stimulate the differentiation and pro-inflammatory actions of CTL in parallel with those that may keep these activities in check, thus potentially maintaining cellular fitness. IL-2 induces a pro-inflammatory gene expression program by regulating the activity of transcription factors such as STAT5, HIF1α and NFIL3 and by boosting protein synthesis. IL-2 stimulates the production of proteins on many levels by regulating levels of amino acid transporters, tRNA synthases, ribosomal subunits, core translational machinery and proteins that coordinate the assembly of translationally competent ribosomal complexes This allows IL-2 to modulate cell phenotype independently of transcriptional networks. Yet, our data revealed that IL-2 equally sustained the expression of proteins that destroy mis-folded proteins. Maintaining these protein degradation pathways may be required to prevent the accumulation of damaged proteins and preserve the cellular fitness of these CTL as they perform the high rates of protein biosynthesis required for rapid cell proliferation and effector function. In a similar way, IL-2 finely tunes the expression of proteins to prevent aberrant immune responses. For example, IL-2 stimulated the expression of 4-1BB, which boosts CTL function, but also regulated the expression of Tim-3

(HAVCR2), which can inhibit CTL function. The ability of IL-2 to control expression of stimulatory and inhibitory receptors would, therefore, control the balanced activity of effector T cells.

One fundamental insight from the current data set is the dominant role for IL-2 in controlling how effector T cells respond to their nutrient environment. We found that IL-2 regulated a diverse repertoire of nutrient transporters including those required for uptake of glucose, iron, methionine, leucine, serine, arginine and glutamine. These amino acids are necessary for protein synthesis and for other critical metabolic pathways. IL-2 also maintained the expression the amino acid sensing pathways mediated by the leucine sensor Sestrin-2 that controls mTORC1 activity. The importance of nutrient supply for effector T cell function is now well recognized, and the effects of IL-2 on nutrient transporter expression, therefore, allow IL-2 to have a major role in co-regulating metabolism and protein expression in effector $CD8^+$ T cells.

One other important discovery was the integration of IL-2 signaling and oxygen sensing signaling pathways. The importance of oxygen sensing in regulating effector T cell function is increasingly recognized. The HIF1 signaling pathway is a crucial regulator of T cell differentiation, and controls the expression of glucose transporters, glycolytic enzymes, chemokine receptors, adhesion molecules and the cytolytic effector molecule, perforin *(21, 43)*. Indeed, elevated HIF1α expression has been linked to enhanced effector $CD8^+$ T cell function *(43)* and loss of PHD protein expression improves the efficacy of effector T cells in the lung to clear tumor metastases *(35)*. The expression of PHDs in T cells in the lung also suppresses

effector T cells to prevent immune-mediated tissue damage *(35)*. Therefore, it is important to understand that IL-2 drives the expression of both HIF1α and PHD2.

In this respect, another novel and intriguing discovery from this study was the convergence of IL-2 and oxygen sensing signaling pathways. An example of this was IL-2 and HIF1 control of the expression of NFIL3, a bZIP family transcriptional repressor in CTL. Previous studies have shown that NFIL3 is important for the development of both NK *(40)* cells and ILC *(42)*. Our finding that NFIL3 is regulated by HIF1 downstream of IL-2 and hypoxia reveals a novel insight into how the expression of this important transcription factor is controlled. It is noteworthy that we found that NFIL3 expression in CTL was strongly downregulated in response to the JAK1/3 inhibitor Tofacitinib. This inhibitor is in clinical use, and our data, thus, gives intriguing insights into the molecular details of how these drugs control immune cell function: for example, it could be important to understand if JAK kinase mediated control of oxygen sensing and HIF1 transcription factors determines NFIL3 expression in NK cells or ILCs.

In summary, the current data highlight the multiple ways in which IL-2/JAK signaling can shape the proteomic landscape of effector T cells to control protein metabolism and other key cellular metabolic programs. These data offer a comprehensive understanding of the impact of IL-2 signaling on effector T cells that explain the powerful immunomodulatory actions of this cytokine.

Materials and Methods

Study plan

This study aimed to define the proteome of *in vitro* generated CTL in the presence or absence of IL-2 and the JAK kinase inhibitor, Tofacitinib. Three biological replicates were used for proteomic studies Each biological replicate was generated from the spleen of one mouse. Mice were age-matched and sex-matched, and were used between 12-15 weeks of age. Where possible, cage-mates were used within each experiment. Other experiments were performed as indicated in the figure legends.

Mice

P14 mice have been described previously *(44)*. Female P14 T cell receptor transgenic mice were used for proteomic studies, and both male and female mice were used for other experiments. Mice with floxed *Hif1a* alleles were crossed with mice expressing Cre recombinase under the control of the Vav promoter to generate mice with deletion of HIF1α in Vav expressing cells. $NFIL3^{-/-}$ mice have been described previously *(40)*. All mice were bred and maintained in compliance with UK Home Office Animals (Scientific Procedures) Act 1986 guidelines.

In vitro cultures of Cytotoxic T Lymphocytes (CTL)

Cytotoxic T Lymphocytes (CTL) were generated as described previously *(24)*. Briefly, $CD8^{+}$ naïve T cells taken from the spleens of mice were activated by triggering of the T cell receptor (TCR) for 48 hours in the presence of 20 ng/ml IL-2 (Proleukin, Novartis) and 2 ng/ml IL-12 (R and D Systems). P14 mice were activated using 100 ng/ml gp-33 peptide of the Lymphocytic Choriomeningitis Virus (LCMV)

and TCR non-transgenic T cells were activated using 0.5μg/ml α-CD3 (BioLegend) and 0.5μg/ml α-CD28 (eBioscience).

After 48 hours of antigen activation, the activated $CD8^+$ cells were removed from TCR stimulation and were then cultured in RPMI 1640 (Life Technologies), with 10% fetal bovine serum (FBS) (Life Technologies), supplemented with 50 units/ml penicillin-G (GIBCO), 50 μg/ml streptomycin (GIBCO), 50 μM β-mercaptoethanol (Sigma-Aldrich) and 20 ng/ml IL-2 (Proleukin, Novartis). CTL were differentiated in IL-2 for 4 days before any 24 hour treatments were performed. Samples were considered biological replicates if CTL were generated from separate spleens.

When required, $CD8^+$ T cells were purified and isolated using the EasySep™ Mouse $CD8^+$ isolation kit (STEMCELL Technologies) as directed by the manufacturer's instructions.

Inhibitors and cell treatments

Cells were treated with 100 nM Tofacitinib (from Selleckchem, Munich, Germany). Where appropriate, cells were treated with DMSO as controls. To deprive cells of IL-2, cells were pelleted, washed in an excess of pre-warmed media lacking IL-2 for 5 minutes before being pelleted and resuspended in pre-warmed media lacking IL-2. For the IL-2 maintained controls, the CTL were subjected to the same washes with 20 ng/ml IL-2 being added back before further culturing.

Proteomic sample processing

Following CTL generation and treatment, CTL were lysed in urea buffer (8 M urea, 50 mM Tris pH 8.0, 1 mM TCEP) with protease (cOmplete™ mini EDTA free, Roche) and phosphatase inhibitors (PhosStop, Roche) at room temperature for 30 minutes. Samples were sonicated, and protein concentration was determined using a BCA assay according to the manufacturer's instructions (Pearce). To reduce samples, 10 mM DTT was added for 30 minutes at room temperature. Following reduction, 50 mM iodoacetimide was added to each sample and incubated for 45 minutes at room temperature in the dark. Samples were then diluted to 4 M urea with 100 mM Tris pH 8.0/1 mM $CaCl_2$. LysC (Wako), reconstituted in 100 mM Tris pH 8.0/1 mM $CaCl_2$, was then added to each sample at a ratio of 50:1 protein:LysC and samples incubated with LysC overnight at 30°C. Samples were then transferred to low bind 15 ml falcon tubes (Eppendorf) and further diluted with 100 mM Tris pH 8.0/1 mM $CaCl_2$ to 0.8M urea. Trypsin (Promega), reconstituted with 100 mM Tris pH 8.0/1 mM $CaCl_2$, was then added to samples at a ratio of 50:1 protein:trypsin, and samples incubated for 8 hours at 30°C. Following digestion, samples were desalted using C18 SepPack cartridges (Waters) and dried down in a SpeedVac (Genevac).

Dried down peptide samples were resuspended 10 mM sodium borate 20% (v/v) acetonitrile, pH 9.3 and fractionated into 16 fractions by strong anion exchange (SAX) chromatography. Fractions were desalted and dried and then resuspended in 1% formic acid and separated by nanoscale C18 reverse phase chromatography (Ultimate 3000 RSLC nano system, Thermo Scientific) before being electrosprayed into the Linear Trap Quadrupole-Orbitrap mass spectrometer (LTQ-Orbitrap Velos Pro; Thermo Scientific). Mass spectrometry was performed by the Proteomics

facility, University of Dundee, UK. Full details of SAX chromatography and LC-MS are in Supplementary Materials and Methods.

Proteomic data processing and analysis

The mass spectrometry data files were processed using MaxQuant version 1.6.0.1 and spectra were mapped to the reviewed UniProtKB mouse protein database and the contaminant database supplied by MaxQuant. Full parameters can be found in Supplemental Materials and Methods. Following processing of the files by MaxQuant, Perseus software implementing the proteome ruler plug-in was used to calculate estimated copy numbers of proteins per cell. This analysis assigns the copy numbers of histones in a diploid mouse cell to the summed peptide intensities of all histones in a sample in order to estimate copy numbers for all identified proteins in the dataset *(26)*. The accuracies of the quantification were annotated based according to the number of peptides and % unique peptides identified for the protein as follows: high: ≥8 peptides detected, minimum of 75% unique peptides; medium: ≥3 peptides detected, a minimum of 50% unique peptides; low: all other peptides.

Data quality was assessed by evaluating peptide intensities for normal distribution, the overlap in protein identification and the correlation of the estimated copy number between replicates. The output from MaxQuant was filtered to remove known contaminants, the proteins identified as part of a reversed protein library, and proteins identified only by a modified site. To evaluate changes to the proteome resulting from loss of IL-2-JAK1/3 signaling, the estimated copy numbers were used to determine the ratio of expression of individual proteins within biological replicates. The significance of these changes was determined by performing a one-sample t-test,

without further adjustment, on the ratios of the treated condition:IL-2 maintained condition. Proteins were defined as significantly regulated if they had a ratio of ≥1.5 or ≤ 0.67 and a *P*-value of ≤0.05.

Western blotting

Cells were lysed in RIPA buffer (50 mM Tris pH 7.4, 1% NP-40, 0.5% sodium deoxycholate, 0.1% SDS, 150 mM NaCl, 2mM EDTA, 50 mM NaF, 20 mM TCEP) with cOmplete™ mini EDTA free protease inhibitor tablets (Roche) for 10 minutes at 4°C. The resulting lysates were sonicated, and then mixed with NuPAGE® LDS sample buffer supplemented with TCEP before being heated to 70°C for 10 minutes. Samples were separated on an SDS-PAGE gel using the Mini-PROTEAN Tetra Cell system. Following separation, proteins were transferred to nitrocellulose membranes (Hybond-C Extra, Amersham). Primary antibodies were detected using HRP-conjugated secondary antibodies (goat anti rabbit, Thermo Scientific #31460; goat anti mouse, Thermo Scientific #31430), and chemiluminescence was detected using X-ray films (Konica) or an Odyssey Fc Imaging System (Licor). Primary antibodies can be found in Supplementary Materials and Methods.

Cell staining and flow cytometry

Cells were stained with saturating concentrations of the following antibodies: CD25 (BD BioScience, clone PC61; or BD Pharmingen, clone 7D4,), CD69 (eBioscience, clone HI.2F3), CD44 (BD Pharmingen, clone IM7), CD62L (BD Pharmingen, MEL-14), CD4 (eBioscience, clone RM4-5), CD8 (BioLegend, clone 53-6.7). Data were acquired on a FACS Verse flow cytometer with FACSuite software (BD Biosciences) or a FACS LSR Fortessa flow cytometer with DIVA software (BD Biosciences).

Viable cells were gated according to their forward- and side-scatter profiles. Data analysis was performed with FlowJo software (Treestar).

RNA extraction and qPCR

RNA was isolated using the Qiagen RNeasy kit and cDNA was generated using the Quantas cDNA synthesis kit. RT-PCR was performed with the SYBRgreen dye (BioRad) on a iCycler iQ™ PCR machine. TBP, CD8 and HPRT were used as the reference gene as indicated in the figure legend. Data were analyzed using the ΔΔCT method. Primers can be found in the Supplementary Materials and Methods.

Glucose uptakes

The measurement of radiolabelled glucose uptake has been described previously *(21)*. Briefly, glucose free RMPI 1640 labelled with 0.5 μCi/ml radiolabelled 2-deoxy-d-[1-3H]glucose (Perkin Elmer) was layered over 500μL of a 1:1 mixture of silicone oil (Sigma Aldrich) and dibutyl phthalate (Sigma Aldrich). Cells ($1x10^6$ per uptake) were added and allowed to take up radiolabelled 2-deoxy-d-[1-3H]glucose for 4 minutes. Cells were lysed in 100 mM NaOH and the radioactivity analyzed using a Beckman LS 6500 Multi-Purpose Scintillation Counter (Beckman Coulter). Assays were performed in duplicate or triplicate per biological replicate. For each biological replicate, data were normalized to the uptake of 2-deoxy-d-[1-3H]glucose in the IL-2 maintained CTL sample.

Lactate output

Lactate measurements were performed as described *(21)*. CTL were resuspended to a concentration of $2x10^6$ cells/ml in RPMI with 10% (v/v) dialyzed serum and

incubated for 4 hours. Following incubation, the supernatants were collected. Lactate concentration was determined using an enzymatic assay in which the oxidation of lactate by lactate dehydrogenase (LDH) is monitored by the change in absorption at 340 nM following reduction of NAD^+ to NADH. To determine lactate concentration, equal volumes of supernatant and master mix (320 mM glycine, 320 mM hydrazine, 2U lactate dehydrogenase and 2.4mM NAD^+) were mixed and incubated for 10 minutes at room temperature. Absorbance of the reactions was then read at 340 nM using a cytofluor II Fluorescence Multi-Well Plate Reader (Perceptive BioSystems). A lactate standard curve was generated and the concentration of lactate in the test samples inferred following data analysis in Prism (GraphPad).

Statistical analyses

Statistical analyses were performed as outlined in the proteomics methods section.

Supplementary Materials

Supplementary Materials and Methods

Fig. S1: Proteomic analysis of CTL

Fig. S2: Proteomic analysis of CTL treated with and without Tofacitinib

Fig. S3: Activation and generation of CTL from $NFIL3^{-/-}$ T cells

Table S1. The proteome of IL-2-maintained and IL-2 deprived CTL.

Table S2. The IL-2 regulated proteome of CTL.

Table S3. The proteome of IL-2-maintained CTL in the presence or absence of Tofacitinib.

References and Notes:

1. W. Liao, J.-X. Lin, W. J. Leonard, Interleukin-2 at the crossroads of effector responses, tolerance, and immunotherapy, *Immunity* **38**, 13–25 (2013).

2. W. Liao, J.-X. Lin, W. J. Leonard, IL-2 family cytokines: new insights into the complex roles of IL-2 as a broad regulator of T helper cell differentiation, *Curr. Opin. Immunol.* **23**, 598–604 (2011).

3. G. Cheng, A. Yu, T. R. Malek, T-cell tolerance and the multi-functional role of IL-2R signaling in T-regulatory cells, *Immunological Reviews* **241**, 63–76 (2011).

4. N. Arenas-Ramirez, J. Woytschak, O. Boyman, Interleukin-2: Biology, Design and Application, *Trends Immunol.* **36**, 763–777 (2015).

5. O. Boyman, J. Sprent, The role of interleukin-2 during homeostasis and activation of the immune system, *Nat. Rev. Immunol.* **12**, 180–190 (2012).

6. S. A. Rosenberg, IL-2: the first effective immunotherapy for human cancer, *J. Immunol.* **192**, 5451–5458 (2014).

7. S. A. Rosenberg, N. P. Restifo, Adoptive cell transfer as personalized immunotherapy for human cancer, *Science* **348**, 62–68 (2015).

8. S. Mitra, A. M. Ring, S. Amarnath, J. B. Spangler, P. Li, W. Ju, S. Fischer, J. Oh, R. Spolski, K. Weiskopf, H. Kohrt, J. E. Foley, S. Rajagopalan, E. O. Long, D. H. Fowler, T. A. Waldmann, K. C. Garcia, W. J. Leonard, Interleukin-2 activity can be fine tuned with engineered receptor signaling clamps, *Immunity* **42**, 826–838 (2015).

9. J. B. Spangler, J. Tomala, V. C. Luca, K. M. Jude, S. Dong, A. M. Ring, P. Votavova, M. Pepper, M. Kovar, K. C. Garcia, Antibodies to Interleukin-2 Elicit Selective T Cell Subset Potentiation through Distinct Conformational Mechanisms, *Immunity* **42**, 815–825 (2015).

10. S. Gillis, K. A. Smith, Long term culture of tumour-specific cytotoxic T cells,

Nature **268**, 154–156 (1977).

11. S. Gillis, P. E. Baker, F. W. Ruscetti, K. A. Smith, Long-term culture of human antigen-specific cytotoxic T-cell lines, *J. Exp. Med.* **148**, 1093–1098 (1978).

12. N. Manjunath, P. Shankar, J. Wan, W. Weninger, M. A. Crowley, K. Hieshima, T. A. Springer, X. Fan, H. Shen, J. Lieberman, U. H. von Andrian, Effector differentiation is not prerequisite for generation of memory cytotoxic T lymphocytes, *J. Clin. Invest.* **108**, 871–878 (2001).

13. V. Kalia, S. Sarkar, S. Subramaniam, W. N. Haining, K. A. Smith, R. Ahmed, Prolonged interleukin-2Ralpha expression on virus-specific CD8+ T cells favors terminal-effector differentiation in vivo, *Immunity* **32**, 91–103 (2010).

14. M. E. Pipkin, J. A. Sacks, F. Cruz-Guilloty, M. G. Lichtenheld, M. J. Bevan, A. Rao, Interleukin-2 and Inflammation Induce Distinct Transcriptional Programs that Promote the Differentiation of Effector Cytolytic T Cells, *Immunity* **32**, 79–90 (2010).

15. J. J. Obar, M. J. Molloy, E. R. Jellison, T. A. Stoklasek, W. Zhang, E. J. Usherwood, L. Lefrancois, CD4+ T cell regulation of CD25 expression controls development of short-lived effector CD8+ T cells in primary and secondary responses, *Proc Natl Acad Sci USA* **107**, 193–198 (2010).

16. T. R. Malek, I. Castro, Interleukin-2 receptor signaling: at the interface between tolerance and immunity, *Immunity* **33**, 153–165 (2010).

17. J. J. O'Shea, D. M. Schwartz, A. V. Villarino, M. Gadina, I. B. McInnes, A. Laurence, The JAK-STAT pathway: impact on human disease and therapeutic intervention, *Annu. Rev. Med.* **66**, 311–328 (2015).

18. D. L. Owen, M. A. Farrar, STAT5 and CD4 (+) T Cell Immunity, *F1000Res* **6**, 32 (2017).

19. G. C. Preston, L. V. Sinclair, A. Kaskar, J. L. Hukelmann, M. N. Navarro, I.

Ferrero, H. R. MacDonald, V. H. Cowling, D. A. Cantrell, Single cell tuning of Myc expression by antigen receptor signal strength and interleukin-2 in T lymphocytes, *EMBO J.* **34**, 2008–2024 (2015).

20. L. V. Sinclair, D. Finlay, C. Feijoo, G. H. Cornish, A. Gray, A. Ager, K. Okkenhaug, T. J. Hagenbeek, H. Spits, D. A. Cantrell, Phosphatidylinositol-3-OH kinase and nutrient-sensing mTOR pathways control T lymphocyte trafficking, *Nat. Immunol.* **9**, 513–521 (2008).

21. D. K. Finlay, E. Rosenzweig, L. V. Sinclair, C. Feijoo-Carnero, J. L. Hukelmann, J. Rolf, A. A. Panteleyev, K. Okkenhaug, D. A. Cantrell, PDK1 regulation of mTOR and hypoxia-inducible factor 1 integrate metabolism and migration of CD8+ T cells, *Journal of Experimental Medicine* **209**, 2441–2453 (2012).

22. J. D. Powell, K. N. Pollizzi, E. B. Heikamp, M. R. Horton, Regulation of Immune Responses by mTOR, *Annu. Rev. Immunol.* **30**, 39–68 (2012).

23. J. L. Hukelmann, K. E. Anderson, L. V. Sinclair, K. M. Grzes, A. B. Murillo, P. T. Hawkins, L. R. Stephens, A. I. Lamond, D. A. Cantrell, The cytotoxic T cell proteome and its shaping by the kinase mTOR, *Nat. Immunol.* **17**, 104–112 (2016).

24. S. H. Ross, C. Rollings, K. E. Anderson, P. T. Hawkins, L. R. Stephens, D. A. Cantrell, Phosphoproteomic Analyses of Interleukin 2 Signaling Reveal Integrated JAK Kinase-Dependent and -Independent Networks in CD8(+) T Cells, *Immunity* **45**, 685–700 (2016).

25. G. H. Cornish, L. V. Sinclair, D. A. Cantrell, Differential regulation of T-cell growth by IL-2 and IL-15, *Blood* **108**, 600–608 (2006).

26. J. R. Wiśniewski, M. Y. Hein, J. Cox, M. Mann, A "proteomic ruler" for protein copy number and concentration estimation without spike-in standards, *Mol. Cell Proteomics* **13**, 3497–3506 (2014).

27. K. A. Smith, D. A. Cantrell, Interleukin 2 regulates its own receptors, *Proc. Natl. Acad. Sci. U.S.A.* **82**, 864–868 (1985).

28. D. K. Dimova, N. J. Dyson, The E2F transcriptional network: old acquaintances with new faces, *Oncogene* **24**, 2810–2826 (2005).

29. M. R. Jenkins, G. M. Griffiths, The synapse and cytolytic machinery of cytotoxic T cells, *Curr. Opin. Immunol.* **22**, 308–313 (2010).

30. L. V. Sinclair, J. Rolf, E. Emslie, Y.-B. Shi, P. M. Taylor, D. A. Cantrell, Control of amino-acid transport by antigen receptors coordinates the metabolic reprogramming essential for T cell differentiation, *Nat. Immunol.* **14**, 500–508 (2013).

31. E. H. Ma, G. Bantug, T. Griss, S. Condotta, R. M. Johnson, B. Samborska, N. Mainolfi, V. Suri, H. Guak, M. L. Balmer, M. J. Verway, T. C. Raissi, H. Tsui, G. Boukhaled, S. Henriques da Costa, C. Frezza, C. M. Krawczyk, A. Friedman, M. Manfredi, M. J. Richer, C. Hess, R. G. Jones, Serine Is an Essential Metabolite for Effector T Cell Expansion, *Cell Metab.* **25**, 345–357 (2017).

32. M. Swamy, S. Pathak, K. M. Grzes, S. Damerow, L. V. Sinclair, D. M. F. Van Aalten, D. A. Cantrell, Glucose and glutamine fuel protein O-GlcNAcylation to control T cell self-renewal and malignancy, *Nat. Immunol.* **17**, 712–720 (2016).

33. R. Geiger, J. C. Rieckmann, T. Wolf, C. Basso, Y. Feng, T. Fuhrer, M. Kogadeeva, P. Picotti, F. Meissner, M. Mann, N. Zamboni, F. Sallusto, A. Lanzavecchia, L-Arginine Modulates T Cell Metabolism and Enhances Survival and Anti-tumor Activity, *Cell* **167**, 829–842.e13 (2016).

34. R. A. Saxton, D. M. Sabatini, mTOR Signaling in Growth, Metabolism, and Disease, *Cell* **168**, 960–976 (2017).

35. D. Clever, R. Roychoudhuri, M. G. Constantinides, M. H. Askenase, M. Sukumar, C. A. Klebanoff, R. L. Eil, H. D. Hickman, Z. Yu, J. H. Pan, D. C. Palmer, A. T.

Phan, J. Goulding, L. Gattinoni, A. W. Goldrath, Y. Belkaid, N. P. Restifo, Oxygen Sensing by T Cells Establishes an Immunologically Tolerant Metastatic Niche, *Cell* **166**, 1117–1131.e14 (2016).

36. M. E. Dowty, M. I. Jesson, S. Ghosh, J. Lee, D. M. Meyer, S. Krishnaswami, N. Kishore, Preclinical to clinical translation of tofacitinib, a Janus kinase inhibitor, in rheumatoid arthritis, *J Pharmacol Exp Ther* **348**, 165–173 (2014).

37. L. M. Lundquist, Efficacy and safety of tofacitinib for treatment of rheumatoid arthritis, *WJO* **5**, 504 (2014).

38. S. Krishnaswami, M. Boy, V. Chow, G. Chan, Safety, tolerability, and pharmacokinetics of single oral doses of tofacitinib, a Janus kinase inhibitor, in healthy volunteers, *Clin Pharmacol Drug Dev* **4**, 83–88 (2015).

39. M. Lamba, R. Wang, T. Fletcher, C. Alvey, J. Kushner, T. C. Stock, Extended-Release Once-Daily Formulation of Tofacitinib: Evaluation of Pharmacokinetics Compared With Immediate-Release Tofacitinib and Impact of Food, *J Clin Pharmacol* **56**, 1362–1371 (2016).

40. D. M. Gascoyne, E. Long, H. Veiga-Fernandes, J. de Boer, O. Williams, B. Seddon, M. Coles, D. Kioussis, H. J. M. Brady, The basic leucine zipper transcription factor E4BP4 is essential for natural killer cell development, *Nat. Immunol.* **10**, 1118–1124 (2009).

41. Y. Motomura, H. Kitamura, A. Hijikata, Y. Matsunaga, K. Matsumoto, H. Inoue, K. Atarashi, S. Hori, H. Watarai, J. Zhu, M. Taniguchi, M. Kubo, The transcription factor E4BP4 regulates the production of IL-10 and IL-13 in CD4+ T cells, *Nat. Immunol.* **12**, 450–459 (2011).

42. W. Xu, R. G. Domingues, D. Fonseca-Pereira, M. Ferreira, H. Ribeiro, S. Lopez-Lastra, Y. Motomura, L. Moreira-Santos, F. Bihl, V. Braud, B. Kee, H. Brady, M. C.

Coles, C. Vosshenrich, M. Kubo, J. P. Di Santo, H. Veiga-Fernandes, NFIL3 orchestrates the emergence of common helper innate lymphoid cell precursors, *Cell Rep* **10**, 2043–2054 (2015).

43. A. L. Doedens, A. T. Phan, M. H. Stradner, J. K. Fujimoto, J. V. Nguyen, E. Yang, R. S. Johnson, A. W. Goldrath, Hypoxia-inducible factors enhance the effector responses of CD8(+) T cells to persistent antigen, *Nat. Immunol.* **14**, 1173–1182 (2013).

44. D. Brändle, K. Brduscha-Riem, A. C. Hayday, M. J. Owen, H. Hengartner, H. Pircher, T cell development and repertoire of mice expressing a single T cell receptor α chain, *Eur. J. Immunol.* **25**, 2650–2655 (1995).

Acknowledgements:

We thank Cantrell group members for their critical discussion of the data, the Biological Resources unit, flow cytometry (M. Lee, A. Whigham, R. Clarke) and Proteomics (D. Lamont and team) at the University of Dundee. **Funding:** Work was supported by the Wellcome Trust (Principal Research Fellowship 097418/Z/11/Z and 205023/Z/16/Z to D.A.C.) and Tenovus Scotland (S.H.R). C.R. was the recipient of a studentship from the Biotechnology and Biological Sciences Research Council (BBSRC) and GlaxoSmithKline.

Author contributions:

C.R. and S.H.R. designed, performed, and analyzed experiments; L.V.S and S.H.R provided training; H.J.M.B supplied mice. D.A.C. and S.H.R. designed the project and wrote the manuscript with intellectual input from C.R.

Data and materials availability:

The proteomics data are available via the ProteomeXchange Consortium (http://proteomecentral.proteomexchange.org) via the PRIDE repository with the dataset identifier PXDxxxxxx.

Figures:

Fig. 1

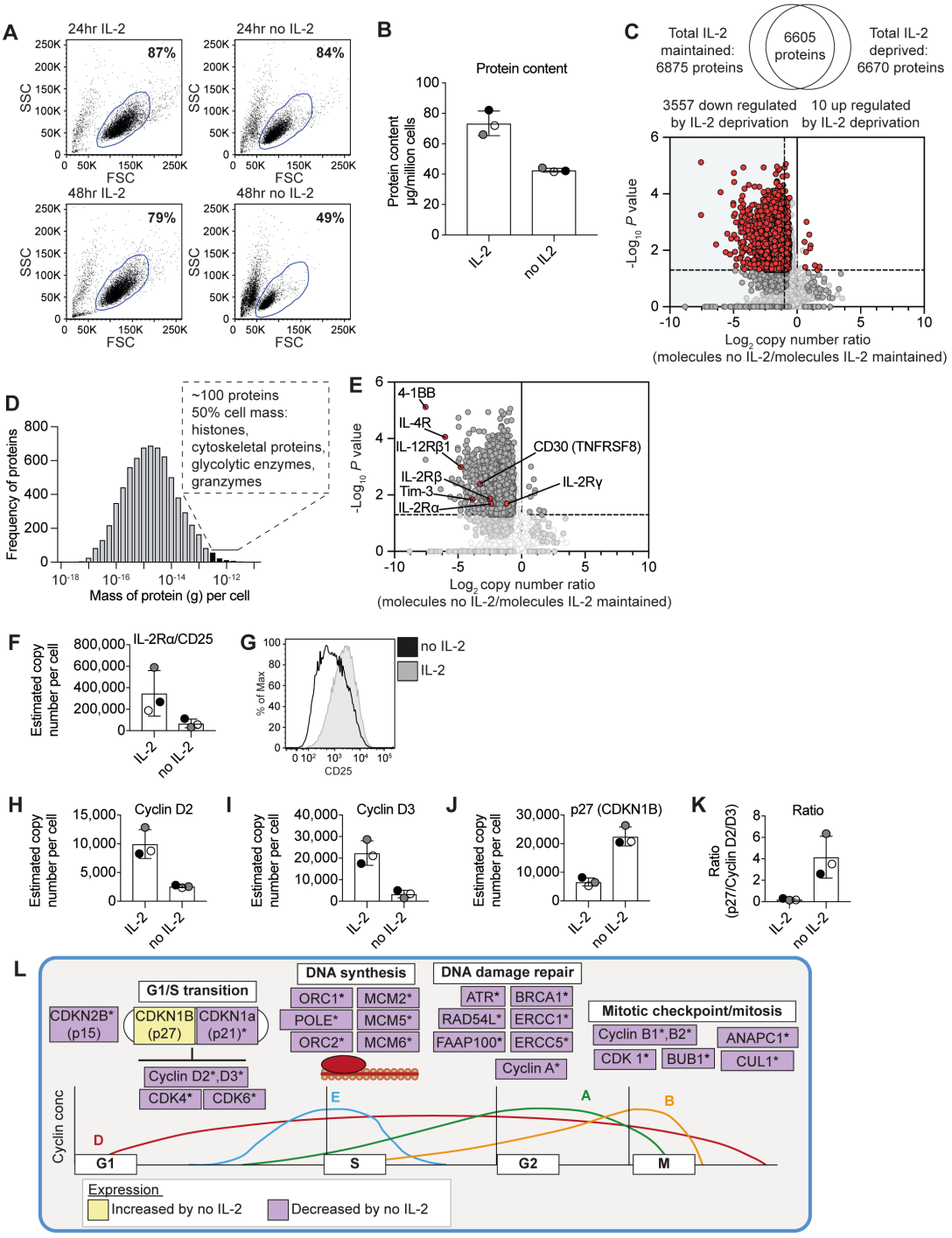

Fig. 1: IL-2 regulation of the CTL proteome.

(**A**) Size and viability of CTL maintained or deprived of IL-2 as judged by flow cytometry forward scatter (FSC) and side scatter (SSC). (**B**) Protein content of IL-2 maintained and IL-2 deprived CTL. (**C**) The Venn diagram shows the commonality of

proteins identified in the proteomic analysis, and the volcano plot shows the ratio of the protein copy number in CTL deprived of IL-2 for 24 hours compared to IL-2-maintained CTL. Proteins significantly changed (one sample students t-test $P < 0.05$) by greater that 1.5-fold are shown in red. The 2-fold downregulation cut-off is indicated by the dashed line. (**D**) Average protein mass frequency per cell - bins containing the proteins that make up ~50% of the total CTL mass are shown in black. (**E**) Volcano plot as in (**C**), with surface receptors shown in red. (**F**) Molecule numbers, estimated from the proteomic data, for the expression of IL-2Rα (CD25). (**G**) Flow cytometric analysis of CD25 cell surface expression. Copy numbers estimated from the proteomic data for Cyclin D2 (CCND2) (**H**), Cyclin D3 (CCDN3) (**I**), and p27 (CDKN1B) (**J**). (**K**) The ratio of p27 to the total sum of Cyclin D2 and Cyclin D3 molecules was calculated and plotted. (**L**) Schematic representation of selected cell cycle proteins, and DNA synthesis and repair enzymes regulated by IL-2. Data show, or are representative of, three biological replicates. In bar charts, data points from biological replicates are color matched, the bar shows the mean and the errors bars show standard deviation.

Fig. 2

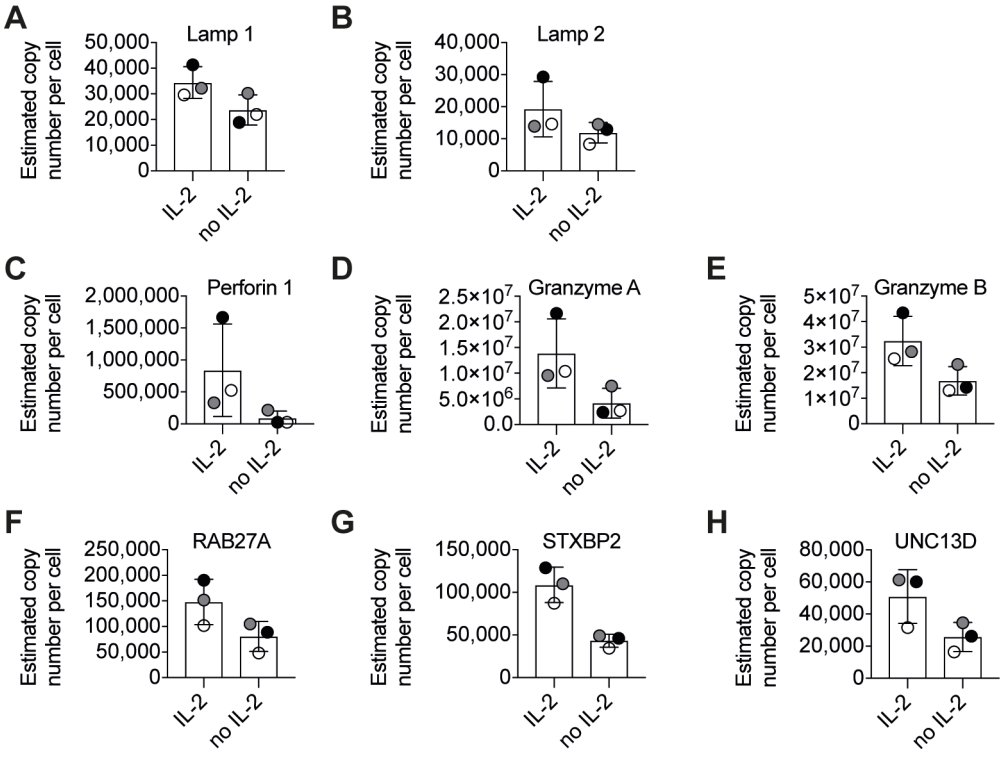

Fig. 2: IL-2 regulation of CTL cytolytic machinery

Copy numbers estimated from the proteomic data for Lamp1 (**A**), Lamp2 (**B**), Perforin 1 (**C**), Granzyme A (**D**), Granzyme B (**E**), RAB27A (**F**), STXBP2 (**G**) and UNC13D (**H**). In graphs, the three biological replicates are color-matched, the bar shows the mean and errors bars show standard deviation.

Fig. 3

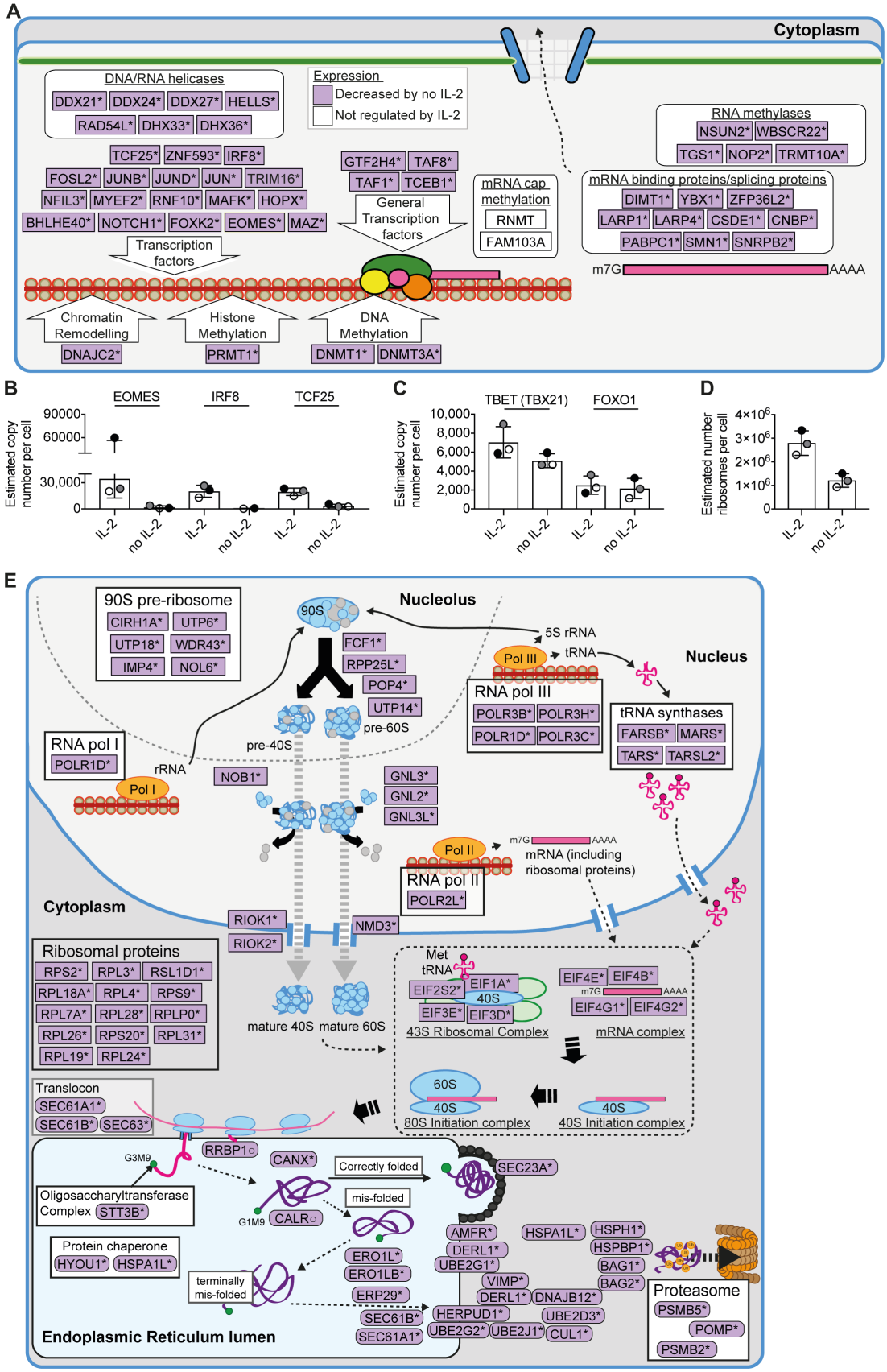
A
Cytoplasm
DNA/RNA helicases
DDX21* DDX24* DDX27* HELLS*
RAD54L* DHX33* DHX36*
Expression
Decreased by no IL-2
Not regulated by IL-2
RNA methylases
NSUN2* WBSCR22*
TGS1* NOP2* TRMT10A*
TCF25* ZNF593* IRF8*
FOSL2* JUNB* JUND* JUN* TRIM16*
NFIL3* MYEF2* RNF10* MAFK* HOPX*
BHLHE40* NOTCH1* FOXK2* EOMES* MAZ*
GTF2H4* TAF8*
TAF1* TCEB1*
General Transcription factors
Transcription factors
mRNA cap methylation
RNMT
FAM103A
mRNA binding proteins/splicing proteins
DIMT1* YBX1* ZFP36L2*
LARP1* LARP4* CSDE1* CNBP*
PABPC1* SMN1* SNRPB2*
m7G AAAA
Chromatin Remodelling
DNAJC2*
Histone Methylation
PRMT1*
DNA Methylation
DNMT1* DNMT3A*
B
EOMES IRF8 TCF25
Estimated copy number per cell
90000
60000
30,000
0
IL-2 no IL-2 IL-2 no IL-2 IL-2 no IL-2
C
TBET (TBX21) FOXO1
Estimated copy number per cell
10,000
8,000
6,000
4,000
2,000
0
IL-2 no IL-2 IL-2 no IL-2
D
Estimated number ribosomes per cell
4×10^6
3×10^6
2×10^6
1×10^6
0
IL-2 no IL-2
E
90S pre-ribosome
CIRH1A* UTP6*
UTP18* WDR43*
IMP4* NOL6*
Nucleolus
90S
FCF1*
RPP25L*
POP4*
UTP14*
pre-60S
pre-40S
5S rRNA
Pol III
tRNA
Nucleus
RNA pol III
POLR3B* POLR3H*
POLR1D* POLR3C*
tRNA synthases
FARSB* MARS*
TARS* TARSL2*
RNA pol I
POLR1D*
rRNA
Pol I
NOB1*
GNL3*
GNL2*
GNL3L*
Pol II
m7G AAAA
mRNA (including ribosomal proteins)
RNA pol II
POLR2L*
Cytoplasm
RIOK1*
RIOK2*
NMD3*
Ribosomal proteins
RPS2* RPL3* RSL1D1*
RPL18A* RPL4* RPS9*
RPL7A* RPL28* RPLP0*
RPL26* RPS20* RPL31*
RPL19* RPL24*
mature 40S mature 60S
Met tRNA
EIF2S2* EIF1A*
40S
EIF3E* EIF3D*
43S Ribosomal Complex
EIF4E* EIF4B*
m7G AAAA
EIF4G1* EIF4G2*
mRNA complex
60S
40S
80S Initiation complex
40S Initiation complex
Translocon
SEC61A1*
SEC61B* SEC63*
G3M9
RRBP1
CANX*
Correctly folded
mis-folded
SEC23A*
Oligosaccharyltransferase Complex STT3B*
G1M9
CALR
Protein chaperone
HYOU1* HSPA1L*
terminally mis-folded
ERO1L*
ERO1LB*
ERP29*
SEC61B*
SEC61A1*
AMFR*
DERL1*
UBE2G1*
VIMP*
DERL1*
DNAJB12*
HERPUD1*
UBE2G2*
UBE2J1*
UBE2D3*
CUL1*
HSPA1L*
HSPH1*
HSPBP1*
BAG1*
BAG2*
Proteasome
PSMB5*
POMP*
PSMB2*
Endoplasmic Reticulum lumen

Fig. 3: IL-2 regulation of gene expression.

(**A**) Schematic representation of selected transcription factors, DNA modifying enzymes and mRNA-binding proteins identified by mass spectrometry in CTL. Proteins downregulated by loss of IL-2 are highlighted in purple. Copy numbers estimated from the proteomic data for Eomesodermin (EOMES), IRF8, TC25 **(B)**, and TBET (TBX21) and FOXO1 (**C**). (**D**) The number of ribosomes per cell was estimated by calculating the median copy number of all the proteins annotated with the KEGG pathway "ribosome" for each biological replicate and each condition and were plotted in a bar chart. (**E**) Schematic representation of selected proteins involved in ribosomal biogenesis, translation and protein processing in the endoplasmic reticulum. Proteins downregulated by loss of IL-2 are highlighted in purple. In graphs, individual data points from the three biological replicates performed for the proteomic analysis are shown and color matched, with the bar showing the mean and the errors bars showing standard deviation of the experiments.

Fig. 4

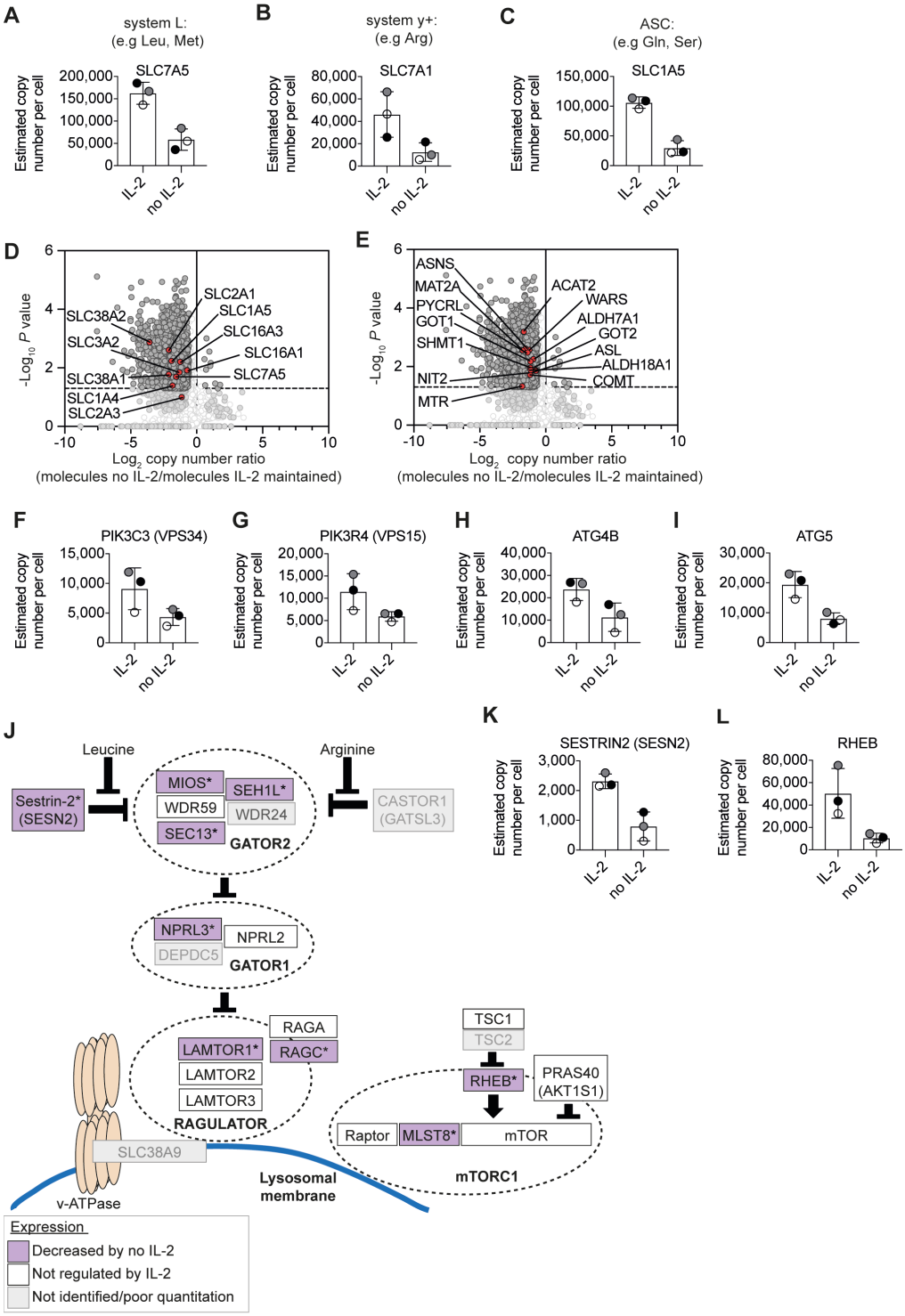

Fig. 4: IL-2 regulation of amino acid uptake and biosynthesis and mTORC1.

Copy numbers estimated from the proteomic data for the amino acid transporter SLC7A5 (**A**), SLC7A1 (**B**) and SLC1A5 (**C**). (**D**) and (**E**) Volcano plots of the IL-2-dependent proteome: ratio of the protein abundance (copy number) in IL-2 deprived

CTL compared to IL-2-maintained CTL is plotted against *P* value (one sample students T-test). Proteins whose ratios are significantly regulated ($P < 0.05$) by greater that 1.5-fold are shown in dark grey, with amino acid transporters highlighted in red in (**D**) and proteins involved in amino acid biosynthesis in (**E**). Bar graphs (**F-I**) show estimated copy numbers calculated using the proteomic data for VPS34 (**F**), VPS15 (**G**), ATG4B (**H**) and ATG5 (**I**). (**J**) Schematic representation of proteins involved in activation of mTORC1 signaling. Proteins downregulated by loss of IL-2 are highlighted in purple. Estimated copy numbers per cell for SESTRIN2 (**K**) and RHEB (**L**). In graphs (**A-C**, **F-I** and **K-L**), individual data points from the three biological replicates performed for the proteomic analysis are shown and color matched, with the bar showing the mean and the errors bars showing standard deviation of the experiments.

Fig. 5

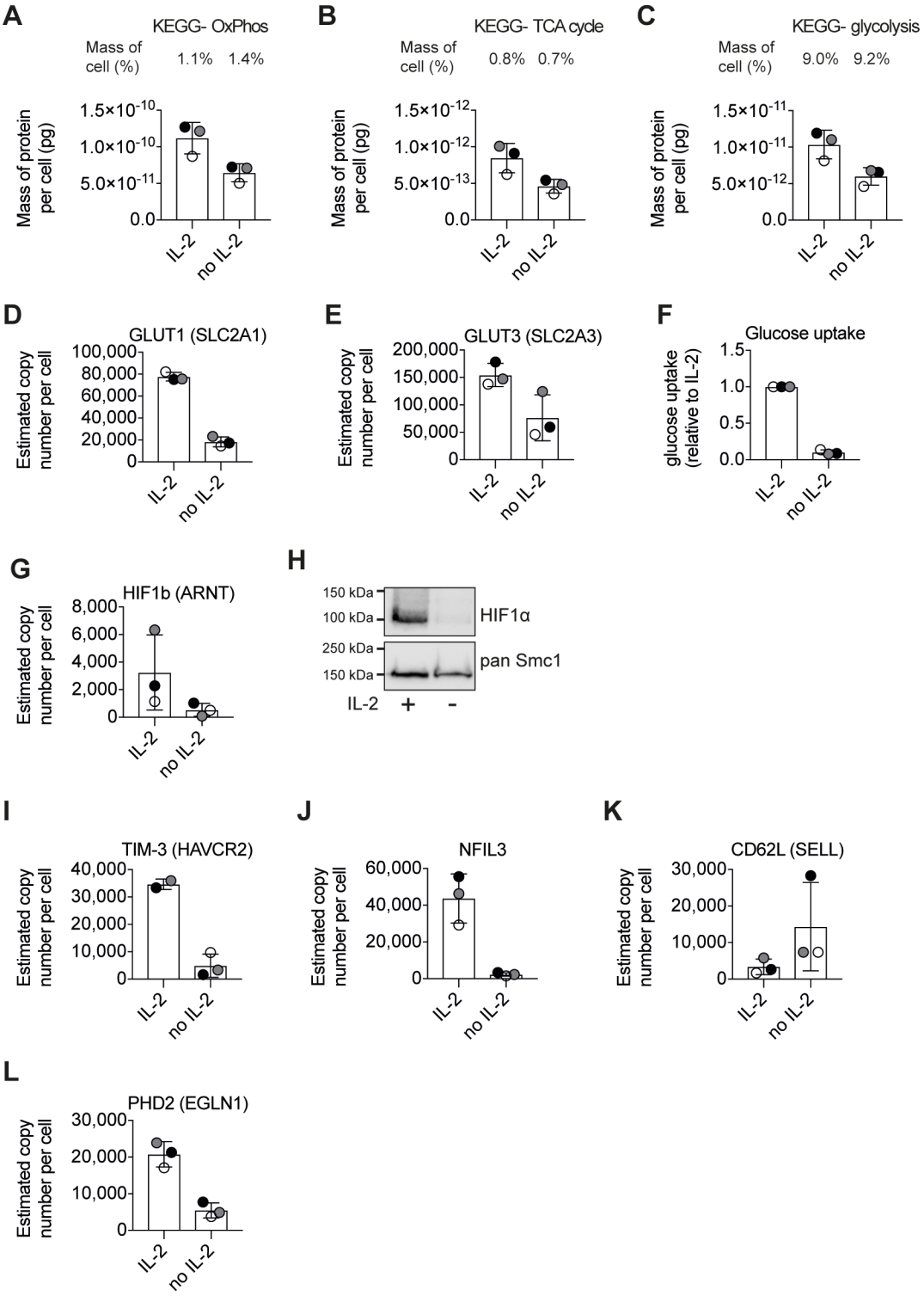

Fig. 5: IL-2 JAK1/3 regulation of cellular energy generation.

(**A-C**) Graphs show the estimated mass of proteins annotated with the KEGG pathway terms "oxidative phosphorylation" (OxPhos) (**A**) "TCA cycle" (**B**) or

"glycolysis" (**C**) per cell in IL-2 maintained and IL-2 deprived CTL. Estimated mass per protein was determined using estimated copy numbers calculated from the proteomic data using the histone ruler method. The bar charts in (**D**-**E**), (**G**) and (**I**-**L**) show estimated copy numbers per cell for GLUT1 (SLC2A1) (**D**), GLUT3 (SLC2A3) (**E**), HIF1β (**G**), TIM-3 (**I**), NFIL3 (**J**), L-selectin (CD62L) (**K**) and PHD2 (**L**). (**F**) Glucose uptake in IL-2 maintained and IL-2 deprived CTL was measured using radiolabeled 2-deoxyglucose. (**H**) HIF1α expression in CTL in the presence and absence of IL-2 was measured by immunoblot (representative of at least 3 biological replicates). In bar charts, individual data points from the three biological replicates are shown and color matched, with the bar showing the mean and the errors bars showing standard deviation of the experiments.

Fig. 6

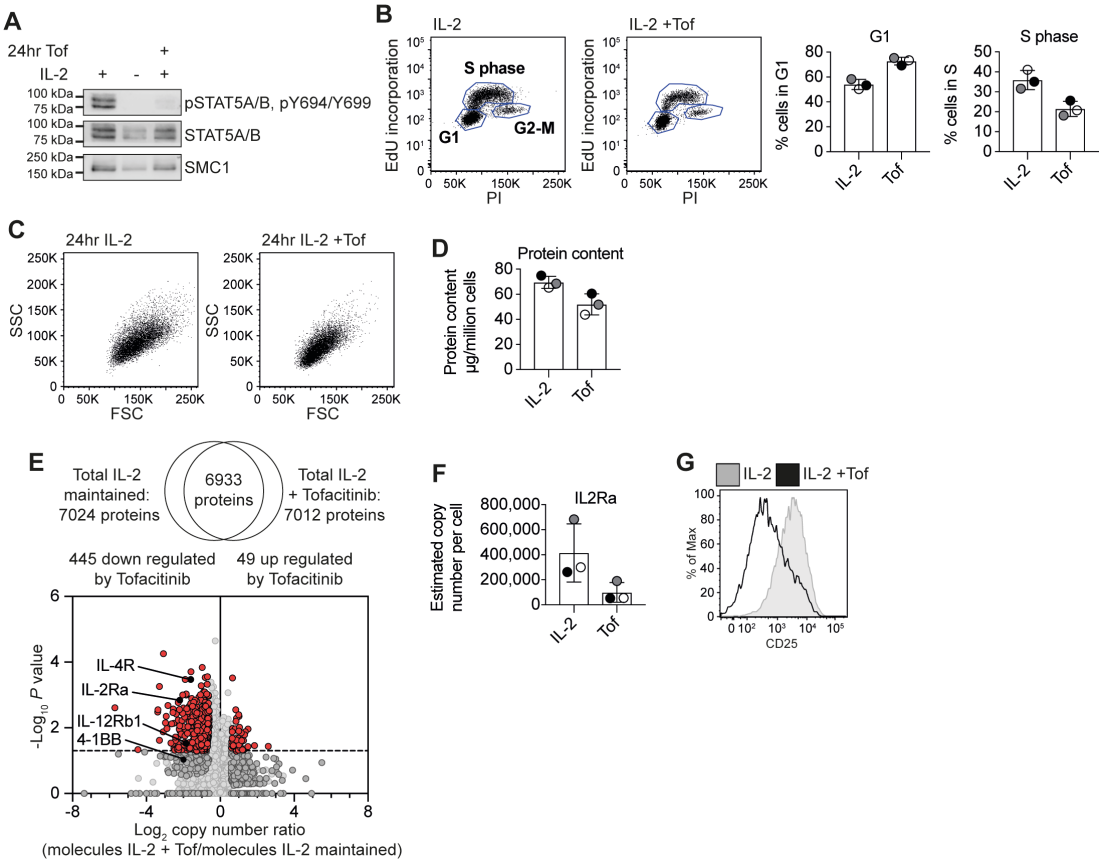

Fig. 6: The impact of Tofacitinib on CTL.

(**A**) Western blot of STAT5A/B phosphorylation in response to 100 nM Tofacitinib treatment. (**B**) Flow cytometric analysis of cell cycle stages using EdU incorporation into DNA. The percentage of CTL identified as in G1 and S are shown alongside. Flow cytometry profiles (**C**) and protein content (**D**) of IL-2 maintained CTL treated with or without Tofacitinib for 24 hours. (**E**) The Venn diagram shows the commonality of proteins identified in the proteomic analysis, and the volcano plot shows the ratio of the protein copy number in IL-2 maintained CTL treated with 100 nM Tofacitinib for 24 hours compared to IL-2-maintained CTL is plotted against *P* value (one sample students t-test). Proteins whose ratios are significantly regulated ($P < 0.05$) by greater that 1.5-fold are shown in red. The regulation of IL-2Rα, IL-4Rα, 4-1BB and IL-12Rβ1 are annotated. CD25 expression as measured by the proteomic

data (**F**) and flow cytometry (**G**) with or without Tofacitinib for 24 hours. The data show, or are representative of, three biological replicates. In bar charts, data points from biological replicates are color matched, the bar shows the mean and the errors bars show standard deviation.

Fig. 7

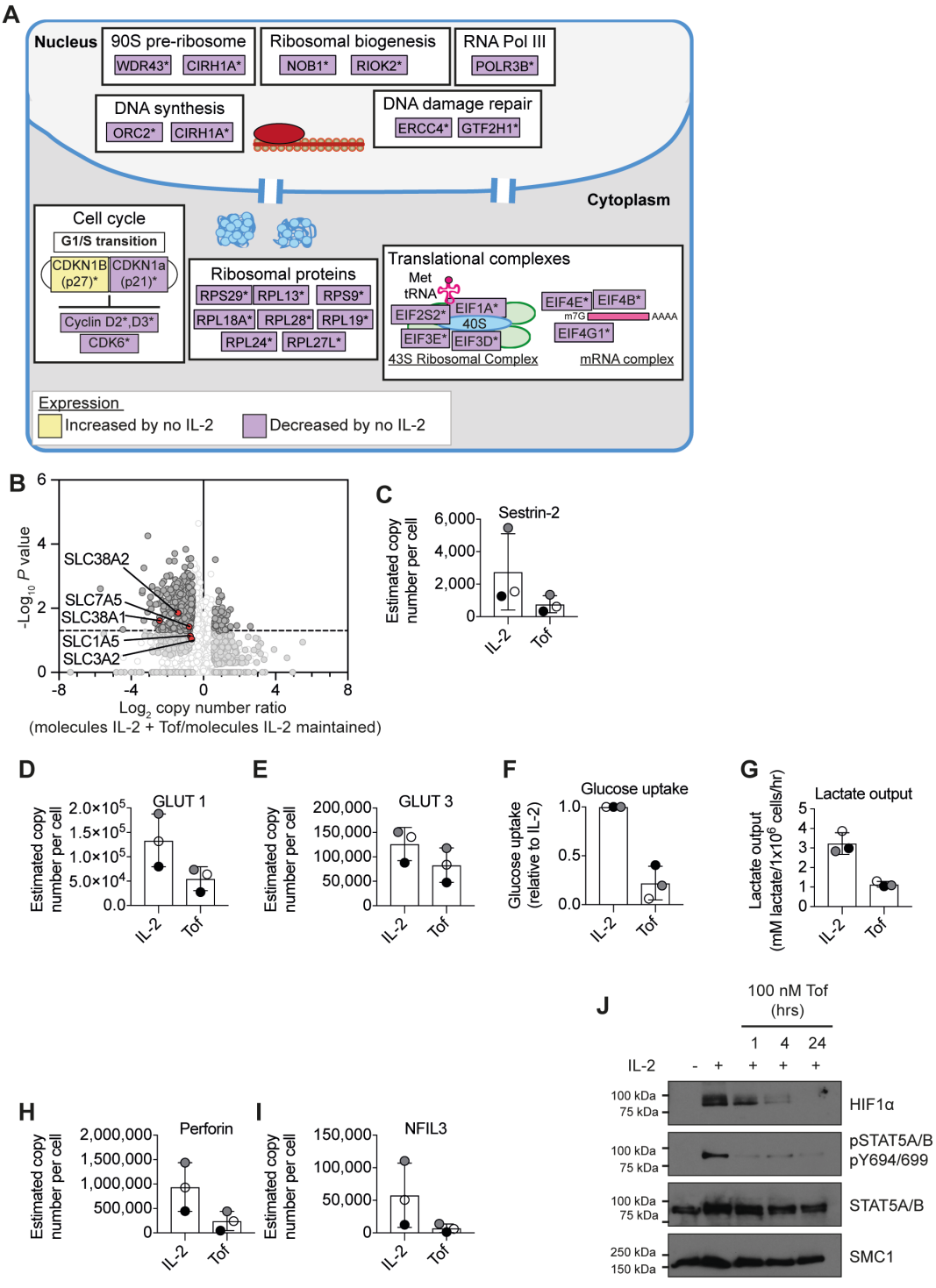

Fig. 7: The Tofacitinib-regulated CTL proteome.

(**A**) Schematic representation of selected molecules regulated by Tofacitinib. (**B**) Volcano plot showing the protein copy number ratio in IL-2 maintained CTL treated with 100 nM Tofacitinib for 24 hours compared to IL-2-maintained CTL,

significantly regulated proteins are shown in dark grey and nutrient transporters are highlighted in red. Estimated copy numbers per cell are shown for SESTRIN2 (**C**), GLUT1 (**D**) and GLUT3 (**E**). (**F**) Uptake of a radiolabelled glucose analogue expressed relative to IL-2. (**G**) Lactate output in IL-2 maintained and Tofacitinib treated CTL. Estimated copy numbers per cell for perforin (**H**) and NFIL3 (**I**). (**J**) Western blot analysis of HIF1α expression in response to 100 nM Tofacitinib. The data show, or are representative of, three biological replicates. In bar charts, data points from biological replicates are color matched, the bar shows the mean and the errors bars show standard deviation.

Fig. 8

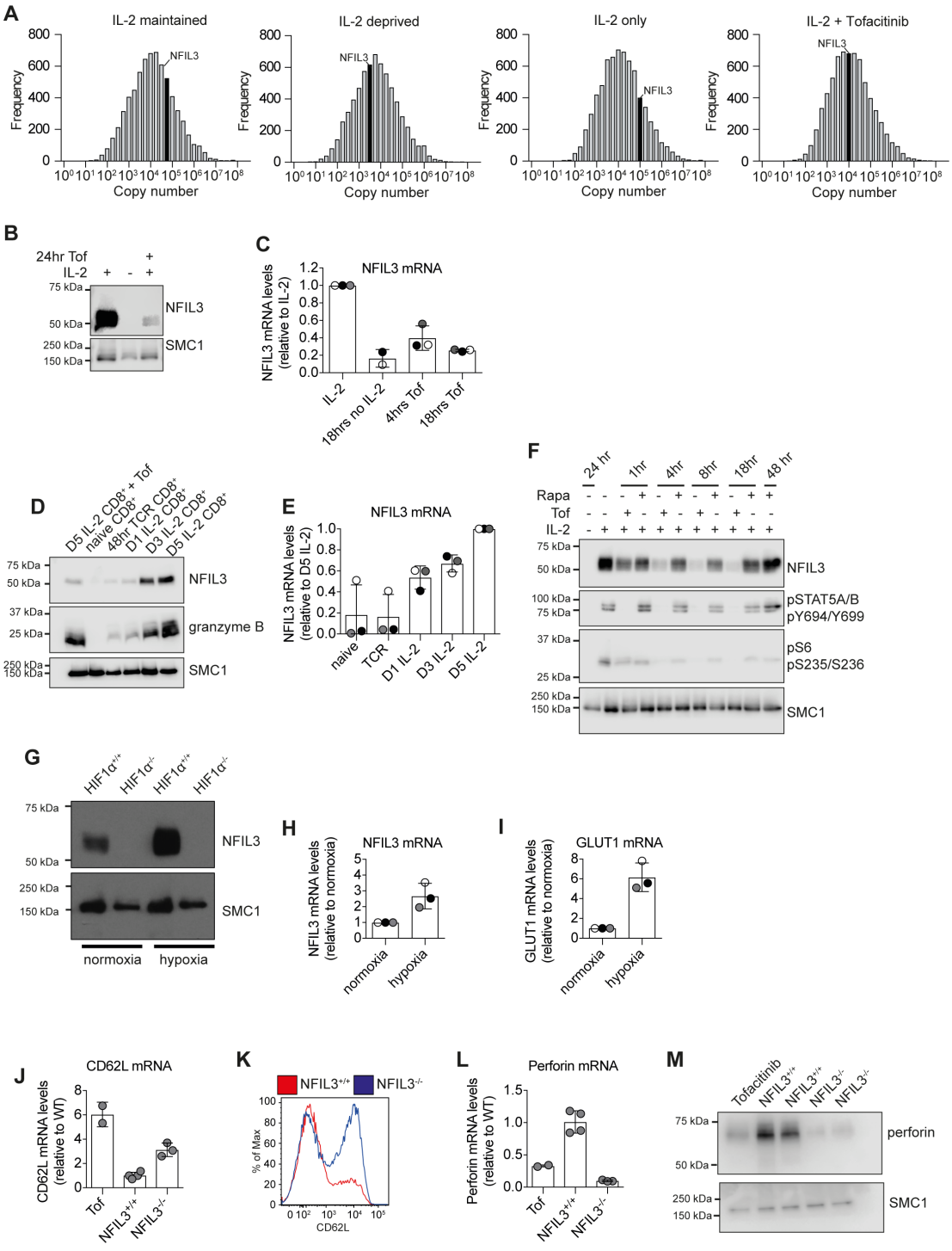

Fig. 8: Regulation of NFIL3 by IL-2-JAK1/3 signaling

(**A**) Average frequency of protein copy numbers per cell calculated from the proteomic datasets: the bin that contains NFIL3 is indicated in black. (**B**) Western blot

analysis of NFIL3 protein expression in CTL following IL-2 deprivation or treatment with 100 nM Tofacitinib. (**C**) Abundance of *Nfil3* mRNA in CTL. Abundance of NFIL3 protein (**D**) and mRNA levels (**E**) in naïve $CD8^+$ T cells, TCR activated $CD8^+$ T cells and CTL activated for 48 hours and then maintained in IL-2 for 1 day (D1), three days (D3) or five days (D5). Analysis of NFIL3 protein abundance in IL-2 maintained CTL treated with 100 nM Tofacitinib or 20 nM rapamycin (**F**) or HIF1α expressing (Vav-Cre^- $HIF1\alpha^{fl/fl}$) and HIF1α deficient (Vav-Cre^+ $HIF1\alpha^{fl/fl}$) CTL maintained in normoxia or switched into hypoxic (1% O_2) conditions for eight hours (**G**). Relative abundance of *Nfil3* (**H**) and *Slc2a3* (**I**) mRNA in CTL maintained in normoxia or switched into 1% O_2 for four hours. Abundance of CD62L mRNA (**J**) and cell-surface protein expression (**K**) in IL-2 maintained $NFIL3^{+/+}$ and $NFIL3^{-/-}$ CTL. Abundance of perforin mRNA (**L**) and protein expression (**M**) in $NFIL3^{+/+}$ and $NFIL3^{-/-}$ CTL. In (**C**), (**H**) and (**I**) the qPCR data were normalized to TBP, in (**E**) to TBP and CD8 and all were expressed relative to (D5) IL-2 maintained CTL in normoxia. In (**J**) and (**L**), mRNA was normalized to HRPT, and data is shown relative to the abundance in $NFIL3^{+/+}$ CTL. Data in (**F**) are representative of two biological replicates; in (**A**)-(**E**) and (**H**)-(**I**) data show, or are representative of, three biological replicates; in (**G**) data are representative of eleven (Vav-Cre^- $HIF1\alpha^{fl/fl}$) and ten (Vav-Cre^+ $HIF1\alpha^{fl/fl}$) biological replicates, four independent experiments; in (**J**)-(**M**) data are representative of four ($NFIL3^{+/+}$) and three ($NFIL3^{-/-}$) biological replicates. Bar charts show data from individual biological replicates, color matched where appropriate, the bar shows the mean and the errors bars show standard deviation.

Supplementary Materials and Methods

Strong anion exchange chromatography (SAX) for peptide fractionation

Peptide samples for proteomic analysis were fractionated using an Ultimate 3000 HPLC equipped with an AS24 strong anion exchange (SAX) column as previously described *(23)*. For the separation, the buffers used were 10 mM sodium borate, pH 9.3 (SAX buffer A) and 10 mM sodium borate, pH 9.3, and 500 mM NaCl (SAX buffer B). Peptide samples were resuspended in 210 µL 10 mM sodium borate 20% (v/v) acetonitrile, pH 9.3 and injected onto the SAX column and separated using an exponential elution gradient starting with Buffer A. In total, 16 peptide fractions were collected and desalted using Sep-pack C18 96 well desalting plates (Waters). Desalted peptides were dried down using a SpeedVac (Genevac).

Liquid Chromatography-Mass Spectrometry

The chromatography buffers were: HPLC Buffer A (0.1% formic acid), HPLC Buffer B (80% acetonitrile, 0.08% formic acid) and HPLC Buffer C (0.1% formic acid). Peptides were loaded onto an Acclaim PepMap100 nanoViper C18 trap column (100 µm inner-diameter, 2cm; Thermo Scientific) in HPLC Buffer C with a constant flow of 5 µl/min. After trap enrichment, peptides were eluted onto an EASY-Spray PepMap RSLC nanoViper, C18, 2 µm, 100 Å column (75 µm, 50 cm; Thermo Scientific) using the following buffer gradient: 2% B (0-3 minutes), 2-40% B (3-128 minutes), 40-98% B (128-130 minutes), 98% B (130-150 minutes), 98-2% B (150-151 minutes), and equilibrated in 2% B (151-180 minutes) at a flow rate of 0.3 µl/minute. The eluting peptide solution was automatically electrosprayed into the coupled Linear Trap Quadrupole-Orbitrap mass spectrometer (LTQ-Orbitrap Velos

Pro; Thermo Scientific) using an Easy-Spray nanoelectrospray ion source at 50˚C and a source voltage of 1.9kV (Thermo Scientific). The mass spectrometer was operated in positive ion mode. Full-scan MS survey spectra (m/z 335–1800) in profile mode were acquired in the Orbitrap with a resolution of 60,000. Data was collected using data-dependent acquisition: the fifteen most intense peptide ions from the preview scan in the Orbitrap were fragmented by collision-induced dissociation (normalized collision energy, 35%; activation Q, 0.250; and activation time, 10 ms) in the LTQ after the accumulation of 5,000 ions. Precursor ion charge state screening was enabled and all unassigned charge states as well as singly charged species were rejected. The lock mass option was enabled for survey scans to improve mass accuracy.

MaxQuant 1.6.0.1 Run Parameters

The following search parameters were used: trypsin and LysC were selected as the proteases; up to two missed cleavages were permitted; the minimum peptide length was set to 6 amino acids; protein N-terminal acetylation, methionine oxidation, glutamine to pyroglutamate, glutamine and asparagine deamidation were selected as variable modifications; carbamindolyation of cysteine residues was set as a fixed modification; MS tolerance of 20 ppm and MS/MS tolerance of 0.5 Da; label free quantification was enabled. False discovery rates (FDRs) were set to 0.01 and based on hits against the reversed sequence database. This cut-off was applied to individual spectra and whole proteins in the MaxQuant output. The match between runs function was enabled. Proteins were quantified on the basis of unique (found only in a specific protein group) and razor peptides (peptides assigned to a specific protein group without being unique to that group) with the re-quantification feature enabled.

Primary antibodies for Western blotting

Membranes were probed with the following primary antibodies: STAT5A/B (CST #9363), STAT5A/B pY694/699 (CST, #9359), NFIL3 (CST #14312), granzyme B (CST #4275), perforin-1 (CST #3693), HIF1α (R and D systems, clone 241809, cat. MAB15361), SMC1 (Bethyl labs, cat. A300-005A), S6 pS235/236 (CST #2211), S6 (CST #2217), S6K pT389 (CST #9205), S6K (CST #9202), AKT pT308 (CST #4056), AKT pS473 (CST #4058), AKT (CST #9272), FOXO1/3A pT24/32 (CST #9464), FOXO1 (CST #9454).

Primers for qPCR

CD8 forward - 5'-GAT ATA AAT CTC CTG TCT GCC CAT C-3'; CD8 reverse - 5'-ATT CAT ACC ACT TGC TTC CTT GC-3'; CD62L forward - 5'-CCT GTA GCC GTC ATG GTC AC-3'; CD62L reverse - 5'-GAA TCA GTA TGG ATC ATC CAT C-3'; GLUT1 forward - 5'-CCA GCA GCA AGA AGG TGA-3'; GLUT1 reverse - 5'-ATG TTT GAT TGT AGA ACT CCT C-3'; HPRT forward - 5'-TGA TCA GTC AAC GGG GGA CA-3'; HPRT reverse - 5'-TTC GAG AGG TCC TTT TCA CCA-3'; NFIL3 forward - 5'-GCG ATG GTA GCC GGA AGT TGC-3'; NFIL3 reverse - 5'-CCT GTG CGG GGC TTT CCT GAG-3'; perforin forward - 5'-CGT CTT GGT GGG ACT TCA G-3'; perforin reverse - 5'-GCA TTC TGA CCG AGT GGC AG-3'; TBP forward - 5'-GGG GAG CTG TGA TGT GAA GT-3'; TBP reverse - 5'-CCA GGA AAT AAT TCT GGC TCA T-3'.

Supplementary Figures and Figure Legends

Fig. S1

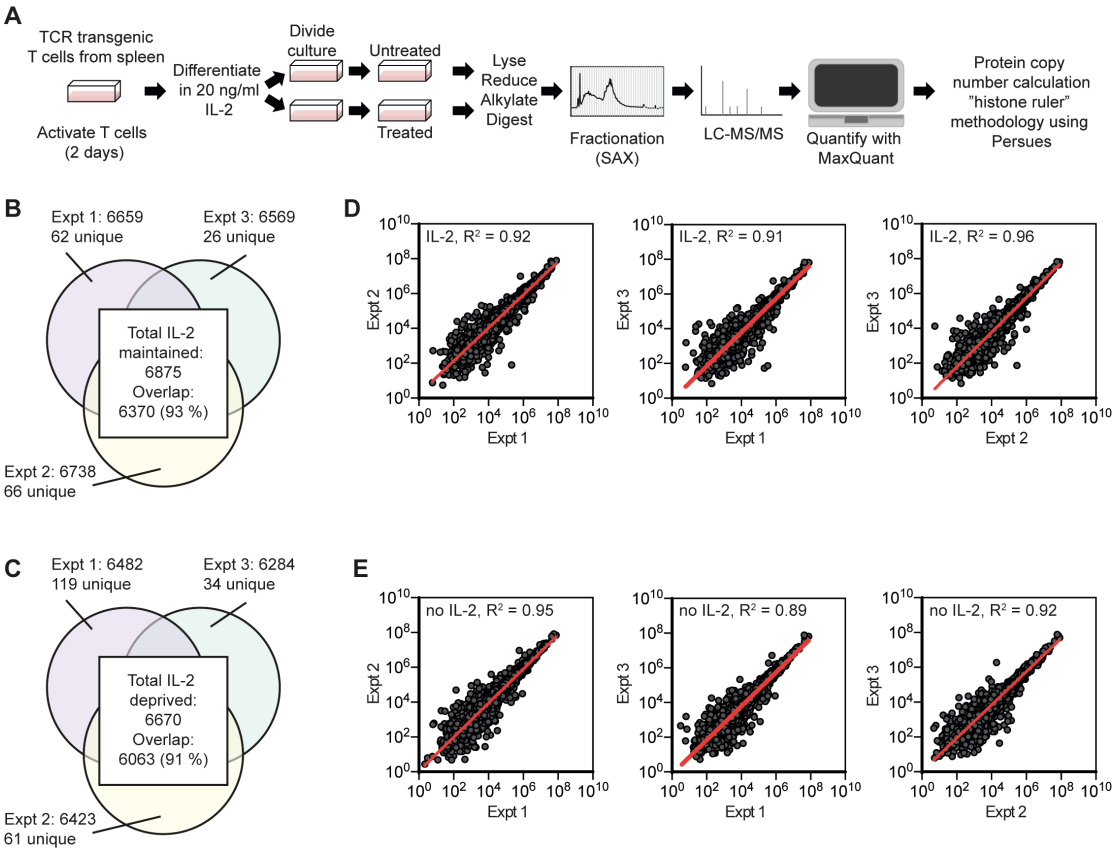

Fig. S1: Proteomic analysis of CTL

(**A**) Experimental workflow for label-free quantitative proteomic analysis of effector cytotoxic T cells (CTL). The overlap in protein identification between biological replicates is shown in the Venn diagrams for IL-2 maintained CTL (**B**) and IL-2 deprived CTL (**C**). The correlation between estimated copy numbers between the biological replicates for IL-2 maintained CTL (**D**) and IL-2 deprived CTL (**E**).

Fig. S2

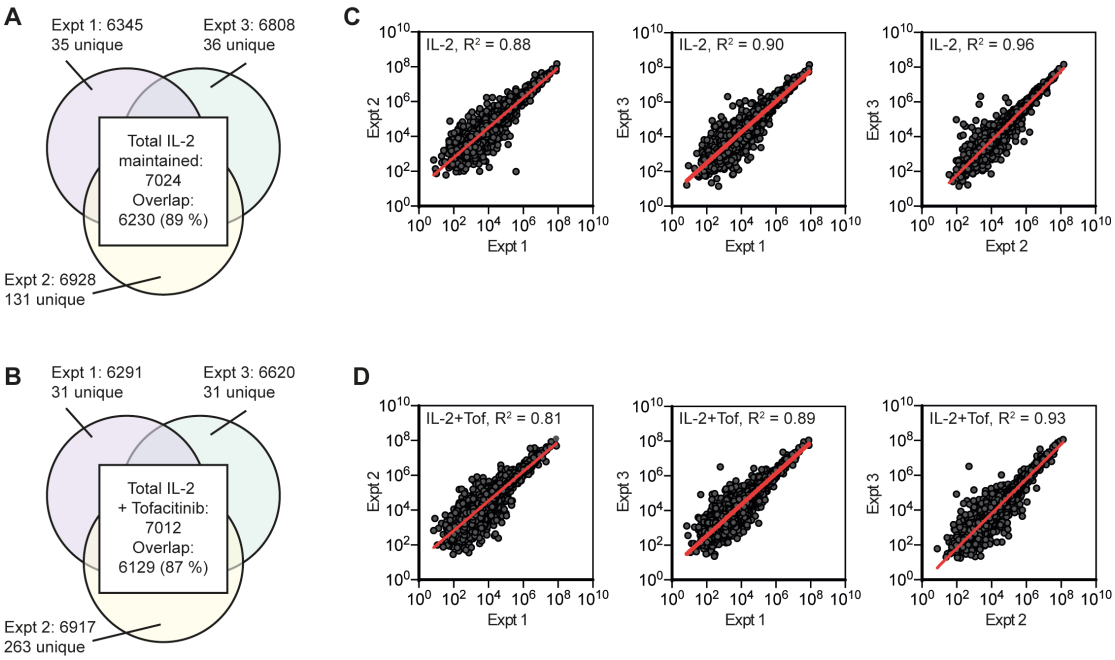

Fig. S2: Proteomic analysis of CTL treated with and without Tofacitinib

The overlap in protein identification between biological replicates is shown in the Venn diagrams for IL-2 maintained CTL (**A**) and IL-2 maintained CTL treated with 100 nM Tofacitinib for 24 hours (**B**). The correlation between estimated copy numbers between the biological replicates for IL-2 maintained CTL (**C**) and IL-2 maintained CTL treated with 100 nM Tofacitinib for 24 hours (**D**).

Fig. S3

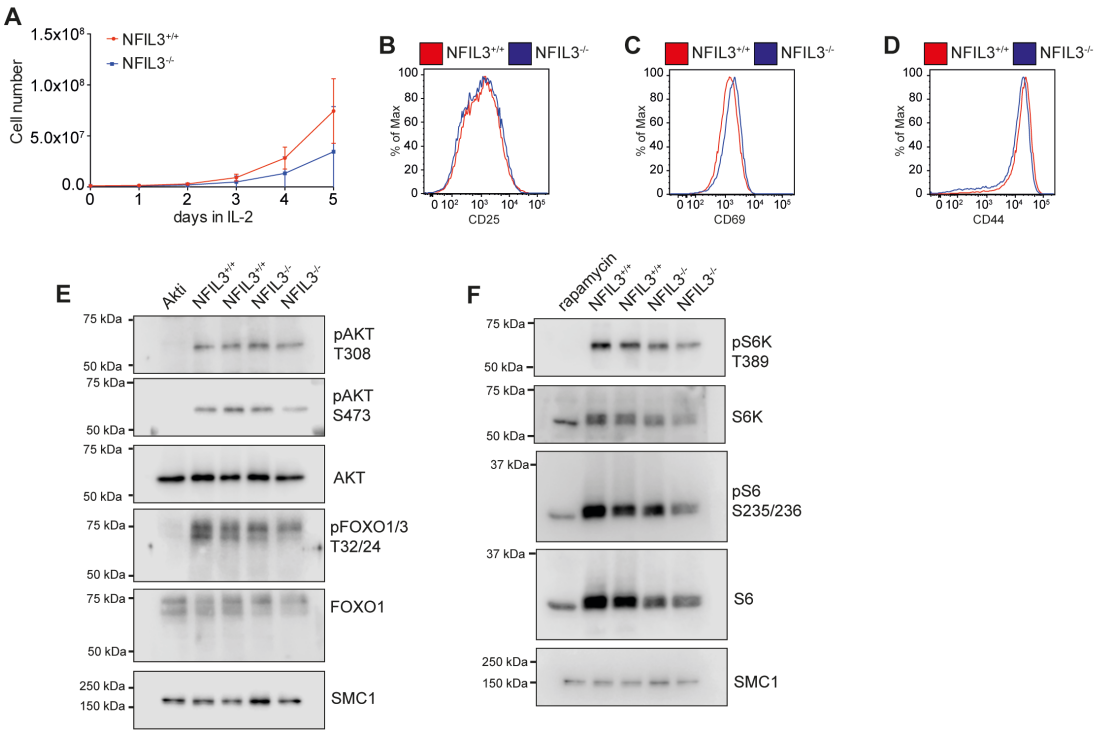

Fig. S3: Activation and generation of CTL from NFIL3$^{-/-}$ T cells

(**A**) T cells from NFIL3$^{+/+}$ and NFIL3$^{-/-}$ mice were TCR-activated for 48 hours. Then, cells were removed from the activation mix and cultured in IL-2 for a further 5 days. The number of cells on each day was counted and graphed. Each point shows the mean number of cells from four biological replicates of NFIL3$^{+/+}$ and three biological replicates of NFIL3$^{-/-}$ CTL cultures. Error bars show standard deviation. (**B-D**) Histogram shows the surface expression of CD25 (**B**), CD69 (**C**) and CD44 (**D**) in IL-2 maintained NFIL3$^{+/+}$ and NFIL3$^{-/-}$ CTL (after 5 days of IL-2). (**E**) and (**F**) western blot analysis of AKT phosphorylation (**E**) and S6K and S6 phosphorylation (**F**) in NFIL3$^{+/+}$ and NFIL3$^{-/-}$ CTL. For controls NFIL3$^{+/+}$ CTL were treated with 1 μM AKTi (AKT inhibitor) (**E**) or 20 nM rapamycin (**F**). In (**A-C** and **E-F**), data are representative of NFIL3$^{+/+}$: four biological replicates; NFIL3$^{-/-}$: three biological replicates. In (**D**), data are representative of two biological replicates per genotype.

Supplemental Table Legends

Table S1. The proteome of IL-2-maintained and IL-2 deprived CTL.

All the proteins identified in three biological replicates of IL-2 maintained CTL (IL-2) and CTL deprived of IL-2 for 24 hours (no IL-2). Copy numbers per cell were calculated using histone ruler methodology and used to calculate the ratio of protein expression (no IL-2/IL-2). Protein ratios increased by 1.5-fold or greater are colored yellow and those decreased by 1.5-fold or greater are highlighted in purple. The significance column shows the *P* values (one sample t-test). Perseus software was used to annotate GO terms and KEGG pathways for the proteins. The second tab shows the peptide identifications for each protein under each condition.

Table S2. The IL-2 regulated proteome of CTL.

Proteins identified in three biological replicates of IL-2 maintained CTL (IL-2) and CTL deprived of IL-2 for 24 hours (no IL-2) where the copy number ratios are statistically (*P* values $\leq$ 0.05, one sample t-test) changed by IL-2 deprivation. In addition, proteins found in two or more replicates in the IL-2 maintained CTL and absent from the IL-2 deprived CTL are shown. Protein ratios increased by 1.5-fold or greater are colored yellow and those decreased by 1.5-fold or greater are highlighted in purple. The significance column shows the *P* values (one sample t-test). Perseus software was used to annotate GO terms and KEGG pathways for the proteins.

Table S3. The proteome of IL-2-maintained CTL in the presence or absence of Tofacitinib.

All the proteins identified in three biological replicates of IL-2 maintained CTL (IL-2) and IL-2 maintained CTL treated with 100 nM Tofacitinib for 24 hours (IL-2 + Tof).

Copy numbers per cell were calculated using histone ruler methodology and used to calculate the ratio of protein expression (IL-2 + Tof/IL-2). Protein ratios increased by 1.5-fold or greater are colored yellow and those decreased by 1.5-fold or greater are highlighted in purple. The significance column shows the *P* values (one sample t-test). Perseus software was used to annotate GO terms and KEGG pathways for the proteins. The second tab shows the peptide identifications for each protein under each condition.